EarthArXiv preprint

Geospatial Foundation Models for forest diversity mapping in structurally complex, species-rich forests

Authors and email addresses

Hormoz Sohrabi[a]* · hsohrabi@modares.ac.ir; hormozsohrabi@gmail.com

Ardalan Daryaei[b] · ardalan.daryaei@boku.ac.at

Ramin Mansour Samaei[c] · ramin.samaee@gmail.com

Sasan Vafaei[c] · sasan.vafaei@gmail.com

Mojdeh Miraki[a] · mojde.miraki@gmail.com

Mahtab Pir Bavaghar[d,e] · m.bavaghar@uok.ac.ir

Parisa Panahi[f] · parisapanahi56@yahoo.com

Rasta Rajaei[a] · rajaei.rasta@gmail.com

Omid Ghorbanzadeh[g] · omid.ghorbanzadeh@plus.ac.at

Gijs van den Dool[h] · gijs.vandendool@gmail.com

Markus Immitzer[b,i] · markus.immitzer@boku.ac.at

Clement Atzberger[i] · clement.atzberger@gmail.com

* Corresponding author

Affiliations

a Department of Forest Science and Engineering, Faculty of Natural Resources, Tarbiat Modares University, Tehran, Iran

b Department of Ecosystem Management, Climate and Biodiversity, Institute of Geomatics, BOKU University, Vienna, Austria

c Office of Forestry and Utilization Affairs, Forest Department, Natural Resources and Watershed Management Organization, Chalus, Iran

d Department of Forestry, Faculty of Natural Resources, University of Kurdistan, Sanandaj, Iran

e Dr. Hedayat Ghazanfari Center for Research and Development of Northern Zagros Forestry, University of Kurdistan, Sanandaj, Iran

f Botany Research Division, Research Institute of Forests and Rangelands, AREEO, Tehran, Iran

g Department of Geoinformatics, University of Salzburg, Salzburg, Austria

h Independent Researcher, Paris, France

i dClimate Labs, New York, United States

This manuscript is a non-peer-reviewed preprint submitted to EarthArXiv. It has been submitted to Geo-spatial Information Science for peer review.

Abstract

Foundation-model satellite embeddings have been proposed as transferable, analysis-ready predictors for Earth Observation, yet their value for biodiversity mapping in forest ecosystems remained unclear. This study addresses three main methodological gaps as one of the first applications of foundation-model embeddings to forest diversity mapping in structurally complex forests: (i) a head-to-head comparison against multi-modal feature stacks and raw data, (ii) the deployment of deep neural networks (DNNs) alongside traditional baselines, and (iii) rigorous spatial cross-validation to mitigate inflated accuracy from spatial autocorrelation. Using National Forest Inventory plots from the Hyrcanian forests in northern Iran as ground truth, we modeled taxonomic α-diversity (Shannon's H', species richness) and structural diversity (diameter at breast height variation). We evaluated annual AlphaEarth Foundation (AEF) and TESSERA embeddings against a comprehensive handcrafted baseline of Sentinel-1/Sentinel-2 time series using a 4-fold spatial block cross-validation repeated across 10 model initializations. Our results indicate that foundation-model embeddings generally produced higher predictive performance than handcrafted feature sets across all ecological targets under spatial cross-validation. The performance was most pronounced for structural diversity, where individual AEF embeddings achieved a median R^2 of 0.62 and an RMSE of 3.34, yielding a substantial reduction in prediction error compared to the top handcrafted baseline (median $R^2 = 0.46$). For Shannon's H' and species richness, embeddings pushed median R^2 values to 0.50 and 0.46, respectively. Although Sentinel-2 spectral data maintained comparable performance in modeling taxonomic indices, embedding models captured structural and canopy-related variation without requiring explicit texture engineering or further fine-tuning. These findings demonstrate that multi-modal foundation embeddings may help improve biodiversity monitoring in structurally complex forests. However, the increased predictive capacity of pretrained embeddings comes at the cost of reduced biophysical interpretability relative to conventional remote-sensing indices.

Keywords: Satellite embeddings; Sentinel-2; Sentinel-1; Shannon diversity; Species richness; AlphaEarth; TESSERA

1. Introduction

Forests are critical life-support systems, but without consistent biodiversity maps, assessments of where and how they are changing remain highly uncertain. The Essential Biodiversity Variables (EBV) were created to help with this by defining a small set of key measures (Jetz et al., 2019). The framework highlights Earth Observation (EO) as a practical way to build indicators that can be updated and compared from national to global scales (Pereira et al., 2013). In this view, satellite products do not replace plots but extend them across space and time with consistent, auditable measurements (Hoffmann et al., 2022; Muise et al., 2024).

Biodiversity has complementary dimensions (Jetz et al., 2019). Taxonomic α-diversity (e.g., richness, Shannon, Simpson, or Hill numbers) summarizes local composition and evenness but differs in sensitivity to rare versus common species, motivating multi-index reporting for interpretability (Jost, 2006). Structural diversity captures variability in forest architecture (diameter, height, layering) that shapes habitat heterogeneity and ecosystem function (MacArthur

and MacArthur, 1961). EO predictors for diversity mapping traditionally rely on handcrafted feature stacks (Kacic and Kuenzer, 2022). From different EO sources, spectral indices (vegetation indices, water and burn proxies, red-edge chlorophyll surrogates, etc), textures, and phenology (amplitude, phase, season length) provide sensitivity to canopy composition and dynamics. Studies show Sentinel-2 (S2) features improve discrimination of tree species and forest communities (Daryaei et al., 2025; Immitzer et al., 2016; Kacic and Kuenzer, 2022; Teshager and Soromessa, 2025). Combining Sentinel-1 (S1) C-band backscatter with S2 often boosts performance, and recent studies in temperate and subtropical forests report significant gains for plant or tree-species diversity mapping using S1+S2 plus topo-climate covariates (Liu et al., 2023; Yang et al., 2022). However, the added value of S1 is not consistent among studies. For example, Lechner et al. (2022) reported only marginal improvements when S1 was combined with dense multi-temporal S2 data for tree-species classification in central Europe.

Leveraging progress in self-supervised learning (SSL), geospatial foundation models (GFMs) are large pretrained models, usually built from annual time series of multi-modal (optical plus SAR) satellite imagery (Brown et al., 2025; Feng et al., 2025). They produce general-purpose embeddings that can be reused for many tasks and often need fewer labels (Lu et al., 2025; Xiao et al., 2025). With a focus on contextual and textural information, Prithvi-EO-2.0 is trained on four-temporal-frame Harmonized Landsat-Sentinel (HLS) image sequences, enabling the model to learn spatial patterns and seasonal dynamics from multi-temporal observations (Szwarcman et al., 2025). Recent reviews list many such models but also note open issues: transfer across regions and years, feature interpretation, and how to test them fairly, avoiding spill-over and other effects inflating the accuracy statistics (Xiao et al., 2025). Due to the novelty of GFMs, biodiversity mapping in species-rich, structurally complex forests is still largely untested, especially in head-to-head comparisons against handcrafted S1/S2 feature baselines.

As species-rich, structurally complex forests, the Hyrcanian forests in northern Iran have served as a testbed for many studies on diversity mapping. Most studies estimating forest diversity have relied on handcrafted remote-sensing features and conventional learners. Early work with Landsat ETM+ related plot-level indices (richness, reciprocal Simpson, and Shannon) to spectral bands and simple spectral transforms using linear or regression-tree models, showing moderate fits while highlighting sensitivity to index choice and scale (Hashemi et al., 2012; Mohammadi and Shataee, 2010). Metric to sub-metric resolution sensors (Pleiades, GeoEye) and machine-learning methods (Generalized Additive Model (GAM), Multivariate Adaptive Regression Spline (MARS), Support Vector Machine (SVM), and Random Forest (RF)) improved local mapping but remained data- and site-specific (Akbari and Kalbi, 2019a, 2019b, 2016). Multi-sensor optical-SAR integration has also been repeatedly tested: Landsat + ALOS/PALSAR (including polarimetric metrics), combined with topographic features, produced the strongest correlations in mountainous terrain, with performance varying by slope strata (Attarchi and Gloaguen, 2018, 2013). S2 vs. Landsat-8 vs. IRS comparisons for tree-species classification generally found NIR/red-edge features to be most informative, but only incremental gains across sensors (Soleimannejad et al., 2019).

More recently, spectral-diversity proxies and tools such as Rao's Quadratic Entropy (RaoQ) via the PaRaVis package (Fathi et al., 2024) have been used to derive α/β-diversity from multi-temporal, multi-index stacks, with Hyrcanian case studies reporting improvements from multi-index and multi-temporal formulations (Fathi et al., 2024), while S2 texture-augmented models still delivered only moderate R^2 for β-diversity in plot-scale tests (Ghaisaryan et

al., 2023). Parallel streams have targeted structural variables: space-borne PCT (TanDEM-X) retrieved diameter at breast height (DBH) variation, and tree density with limited explanatory power, indicating promise but clear room for improvement (Poorazimy et al., 2023). Airborne laser scanning (ALS)/digital aerial photogrammetry (DAP) fusion improved diversity estimates in uneven-aged stands (Mohammadi et al., 2020); and Global Ecosystem Dynamics Investigation (GEDI)-based modeling advanced stand attributes such as basal area, volume, and density at scale (Sohrabi and Akhavan, 2026).

Relative to the mentioned studies, four gaps stand out:

- Applications of foundation-model embeddings to forest diversity mapping remain limited; this work is the first application of embeddings in these species-rich, structurally complex systems.
- Many evaluations rely on random or partial spatial cross-validation, risking inflating derived accuracy metrics in spatially autocorrelated forests (Ghaisaryan et al., 2023; Mohammadi et al., 2011; Mohammadi and Shataee, 2010). In contrast, this study adopts a rigorous spatial block cross-validation framework with geographically separated training and testing regions, thereby providing more realistic estimates of model transferability and predictive performance.
- While structural mapping is advancing with PCT, ALS/DAP, and GEDI, these pipelines either show limited predictive strength for DBH variation or depend on sensors not universally available wall-to-wall; few works quantify calibration, uncertainty, or error stratification across stand conditions (Mohammadi et al., 2011; Poorazimy et al., 2023; Sohrabi and Akhavan, 2026). This study addresses these limitations by evaluating structural diversity using globally available satellite observations, while explicitly quantifying predictive uncertainty, calibration, and error stratification across gradients in stand structure and stem density.
- Almost all Hyrcanian studies used traditional machine-learning methods (e.g., linear models, RF, SVM, GAM/MARS) and small, single-district datasets (for example: Attarchi and Gloaguen, 2018; Fathi et al., 2024; Ghaisaryan et al., 2023; Mohammadi et al., 2011; Mohammadi and Shataee, 2010; Sohrabi and Akhavan, 2026). In contrast, the present study applies deep neural networks (DNNs) to a large, standardized National Forest Inventory (NFI) dataset spanning the entire Hyrcanian forest belt.

Building on these insights, a controlled benchmark is presented for the structurally complex, species-rich Hyrcanian forests in northern Iran. Beyond a head-to-head evaluation, the study introduces and operationalizes a novel embedding-based pipeline for forest diversity mapping, constituting a first application of foundation-model embeddings to this problem. The central question addressed is whether foundation-model embeddings can estimate forest diversity and can outperform remote-sensing features for taxonomic and structural indicators; accordingly, a comparative assessment is also conducted against handcrafted S1/S2 stacks (spectral, phenology, textures, and SAR backscatter/NDI). NFI plots were used to calculate species Richness, Shannon's H′, and structural diversity (DBH variation, as standard deviation). Separate DNNs were trained for each target. Spatially explicit cross-validation was used to keep training and test areas apart, and accuracy, calibration, and uncertainty were reported. Results were compared with recent deep-learning studies on biodiversity mapping. To the best of current knowledge, foundation-model embeddings have not yet been used for forest diversity mapping. This work illustrates a new, embedding-based

workflow for mapping diversity in species-rich, structurally complex forests, while carefully evaluating where embeddings add value over handcrafted S1/2 features.

2. Materials and Methods

2.1. Study Area & Field Data

Stretching along the south shore of the Caspian Sea, the Hyrcanian forests form a globally significant ecoregion with deep evolutionary roots and marked ecological complexity. The belt runs for roughly 800 km between the northern slopes of the Alborz Mountains and the Caspian coast (Fig. 1A), and varies from about 20 to 70 km in width (Ramezani et al., 2016; Sagheb Talebi et al., 2014). Elevations range from sea level to >2,800 m (Fig. 1B), producing strong environmental gradients and a mosaic of forest types. Spanning more than 2 million ha across Gilan, Mazandaran, and Golestan provinces in Iran, the region represents a remnant of Tertiary deciduous forests that persisted through glacial–interglacial cycles (Akhani et al., 2010; Ramezani et al., 2008; Sagheb Talebi et al., 2014). Classic Arcto-Tertiary relics (*Pterocarya fraxinifolia*, *Parrotia persica*, *Zelkova carpinifolia*) still occur here, having survived Quaternary cooling in Hyrcanian refugia after disappearing from much of Europe (Homami Totmaj et al., 2021; Ramezani et al., 2008). Steep terrain, intricate stand structures, and rapidly changing atmospheric conditions complicate ecological monitoring, making the Hyrcanian both challenging and crucial for testing satellite-based and machine-learning approaches to biomass and diversity mapping (Müller, 2019; Sohrabi, 2025).

Field data came from the recent (2023) NFI (6^{th} NFI). Circular plots of 1,000 m² were placed on a 1 × 5 km² systematic grid (Fig. 1C) across the entire Hyrcanian belt. The 6^{th} NFI is the first opportunity to evaluate diversity models across the full ecoregion rather than within a single forest district. In each plot, all trees with DBH > 12.5 cm were measured, and species were recorded. Based on regional patterns showing diversity hotspots from sea level to around 1,000 m, plots between sea level and 1,500 m were selected; the upper bound provided a buffer. From the NFI database, plot tables included tree species and DBH. Plots with fewer than five trees were excluded to avoid highly unstable Shannon/Richness estimates and extreme discrete-count behavior. After filtering, 1,304 plots remained for analysis. Three plot-level response variables were then computed: Shannon's H′ (shannon_H) (Shannon, 1948), species richness (Gotelli and Colwell, 2001), and structural diversity as the standard deviation of DBH (dbh_std) (Hoffmann et al., 2022).

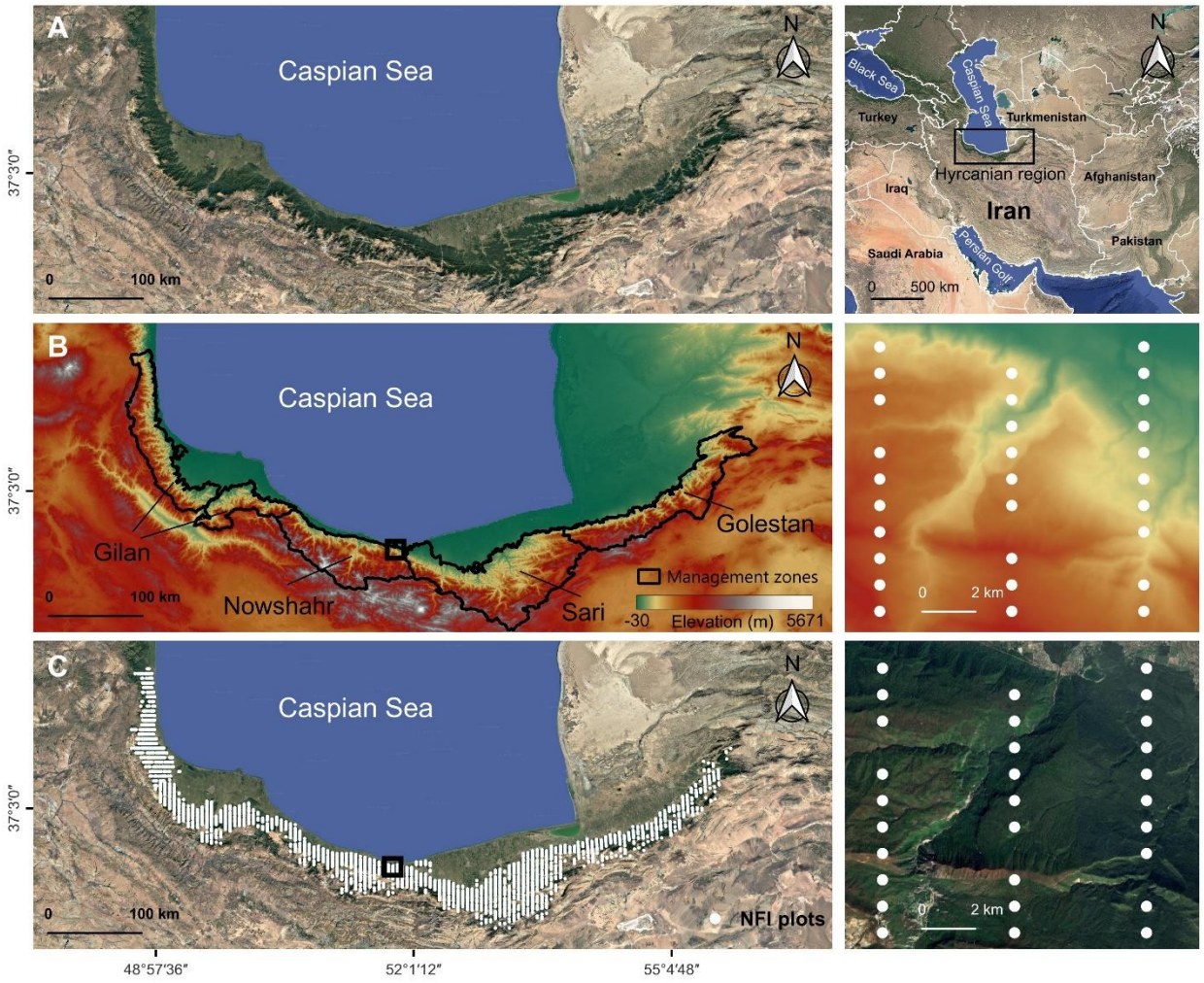

Fig. 1. Study area. (A) Iran with the Hyrcanian forest belt; (B) elevation (m a.s.l.) across the Hyrcanian Management Zones; (C) National Forest Inventory (NFI) plots.

Relationships among three plot-level response variables across NFI plots are illustrated in Fig. 2. The left panel shows a relatively strong positive relationship between species richness and Shannon diversity, indicating that plots containing a greater number of tree species generally exhibit higher taxonomic diversity. In contrast, the middle and right panels reveal weak relationships between structural diversity and the two taxonomic indicators, suggesting that variation in tree-size heterogeneity is largely independent of species composition and richness. These patterns demonstrate that taxonomic and structural diversity capture complementary dimensions of forest biodiversity and therefore should not be considered interchangeable indicators.

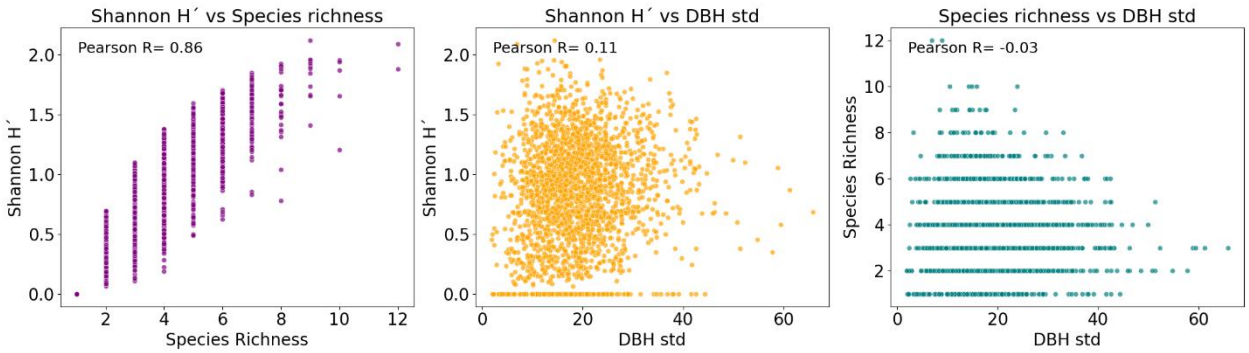

Fig. 2. Pairwise relationships among taxonomic and structural diversity indicators in the Hyrcanian National Forest Inventory plots.

2.2. Sentinel-1/Sentinel-2 Data and Preprocessing

A 16-day time series of C-band SAR from S1 was drawn from COPERNICUS/S1_GRD in IW mode with dual polarization (VV, VH) for both ascending and descending passes for the same year of NFI data collection (2023). Processing converted dB to linear backscatter, applied a light speckle filter, and performed DEM-based radiometric terrain correction (RTC) to Gamma⁰ using SRTM 30 m; local and projected incidence angles were also computed. From the mosaics, Gamma⁰ backscatter was retained (VV_ASC/DESC, VH_ASC/DESC). Two polarimetric normalized-difference summaries were added: the normalized difference index (NDI) of medians (S1_ndi) and the NDI of standard deviations (S1_ndi_sd) (Mohite et al., 2020). These indices quantify the relative difference between VV and VH backscatter responses while normalizing for their overall magnitude. Because VV and VH polarizations interact differently with vegetation structure, the indices provide information on canopy density, vegetation complexity, and scattering mechanisms. Higher absolute differences between VV and VH often reflect variations in forest structure, biomass, and canopy organization. The normalized-difference formulation was selected because it is dimensionless, reduces sensitivity to overall signal strength, and highlights the relative contribution of the two polarizations, making it easier to compare across sites and environmental conditions.

A pre-Gray-Level Co-occurrence Matrix (GLCM) workflow first built a single ND image per pass, fused ASC/DESC using median to reduce aspect bias, and computed GLCM metrics with a 3×3 window: contrast, dissimilarity, entropy, and homogeneity, which were retained as ND_CON, ND_DIS, ND_ENT, and ND_HOM.

$$\text{Eq. (1)} \qquad S1\_ndi = \frac{VV\_med - VH\_med}{VV\_med + VH\_med}$$

$$\text{Eq. (2)} \qquad S1\_ndi\_sd = \frac{VV\_sd - VH\_sd}{VV\_sd + VH\_sd}$$

where VV_med and VH_med are the median VV and VH backscatter values, respectively, and VV_sd and VH_sd are the corresponding standard deviations.

Surface reflectance from a 16-day composite of S2 was obtained from S2_SR_HARMONIZED over the same dates, filtered to a cloudy pixel percentage ≤ 30, and cloud/shadow masked with the Scene Classification Layer (excluding classes 0, 1, 3, 8, 9, 10, 11). The Enhanced Vegetation Index (EVI) was computed from B8, B4, and B2 using the standard coefficients (Huete et al., 2002). EVI was selected instead of NDVI because it is less prone to saturation in densely vegetated forests and is more sensitive to variations in canopy structure and biomass, making it particularly suitable for the closed-canopy conditions of the Hyrcanian forests. GLCM textures (3 × 3 window) were derived from the EVI layer, and four texture metrics, contrast (EVI_CON), dissimilarity (EVI_DIS), entropy (EVI_ENT), and homogeneity (EVI_HOM), were retained for subsequent analyses. RaoQ was computed within a 3×3 window using the quadratic-entropy identity under squared-Euclidean distance (twice the sum of local per-band variances), yielding S2_RaoQ.

Eq. (3) $$EVI = G \times \frac{NIR - RED}{NIR + C_1 \times RED - C_2 \times Blue + L}$$

where G=2.5, C1=6, C2=7.5, and L=1. For S2 imagery, NIR, Red, and Blue correspond to bands B8, B4, and B2, respectively.

2.3. AlphaEarth Embeddings (AEF)

The AEF dataset offers a new way to condense EO information by delivering globally consistent embedding fields. Instead of handling many separate products in space and time, AEF produces task-agnostic, 10-m embeddings composed of 64-dimensional feature vectors that fuse multiple data streams using a patch-based approach: multispectral optics (S2; Landsat 8/9) and C/L-band radar (S1; ALOS PALSAR). As target sources, the models use lidar-derived structure (GEDI metrics), climate reanalysis (ERA5-Land), topography (Copernicus DEM), gravity anomalies (GRACE), and land cover (e.g., NLCD). AEF also projects geotagged text sources (e.g., Wikipedia, GBIF records) into the same feature space. The result is a continuous, globally harmonized representation that helps bridge gaps in sparse or unevenly distributed observations (Brown et al., 2025a). Inputs feeding the embedding do not need to be perfectly time-aligned. For this study, the global annual release for 2023 was used. The annual 2023 AEF embeddings were retrieved from the Google Earth Engine Data Catalog, which provides global 10-m embedding layers generated by the AlphaEarth Foundation model (Brown et al., 2025b).

2.4. TESSERA Embeddings

The TESSERA (Temporal Embeddings of Surface Spectra for Earth Representation and Analysis) framework is an open-source satellite remote-sensing foundation model designed to overcome the challenges of sparse, irregular, and cloud-obscured satellite time series (Feng et al., 2026). Developed at the University of Cambridge based on the concept of spectral temporal Barlow Twins (Atzberger et al., 2025; Lisaius et al., 2026), TESSERA produces 128-dimensional latent representations at a 10-meter global resolution. The pixel-based model utilizes a self-supervised

learning strategy, specifically employing the Barlow Twins loss (Zbontar et al., 2021) to enforce invariance across augmentations, i.e., 40 randomly sampled cloud-free observations from the same location. This allows the model to become agnostic to missing temporal data while maintaining a consistent representation of the land surface (Feng et al., 2026). Structurally, TESSERA employs a dual-branch Transformer-based encoder: one branch dedicated to S1 SAR (VV and VH polarizations) and another to S2 MSI (10 spectral bands). By preserving spectral-temporal phenological signals, which are typically discarded in traditional compositing methods, TESSERA provides high-fidelity representations of ecosystem dynamics. These "analysis-ready" annual embeddings enable state-of-the-art performance in complex downstream ecological tasks, such as canopy height modeling and crop identification, even with very limited labeled training data (Feng et al., 2026). Contrary to patch-based approaches such as AEF of Prithvi, the TESSERA team advises users to derive textural and contextual information after the pre-training to keep this information disentangled. Annual 2023 TESSERA embeddings were obtained from the University of Cambridge TESSERA project following a formal embedding request submitted through the GeoTessera repository. The requested embedding tiles were subsequently downloaded and processed using the GeoTessera framework (Feng et al., 2026).

2.5. Uniform Manifold Approximation and Projection

To further explore how different predictor representations organize ecological information, we projected the handcrafted S1/S2 features and the two foundation-model embedding spaces into 2D using Uniform Manifold Approximation and Projection (UMAP, n_neighbors = 30, min_dist = 0.05, n_components = 2, random_state = 100). Although UMAP does not provide a quantitative assessment of predictive performance, it offers a useful visualization of neighborhood relationships in the original high-dimensional feature space

2.6. Feature Sets

All remote-sensing layers were clipped to the forest mask of the study area and harmonized to a common spatial grid. A joint validity mask was applied to retain only pixels with complete observations across all contributing S1/S2 time-series datasets, and the resulting layers were sampled at NFI plot locations. To systematically evaluate the contribution of different remote-sensing data sources and feature-engineering strategies, twelve distinct predictor sets were constructed (Table 1).

The first group comprised S1 radar-based configurations: S1 Backscatter, including VV and VH backscatter coefficients; S1 Backscatter + NDI, which additionally incorporated radar-derived NDI; S1 Textures, consisting of GLCM texture metrics derived from S1 imagery; and S1 Backscatter + NDI + Textures, representing the complete S1 feature stack.

The second group focused on S2 optical predictors. S2 Spectral included the multispectral bands (B2–B8A, B11, and B12). S2 Spectral + EVI + RaoQ extended the spectral stack with the EVI and RaoQ, representing spectral diversity and heterogeneity. EVI Textures consisted exclusively of texture metrics derived from multi-temporal EVI imagery. S2 Full combined all S2 spectral, vegetation-index, diversity, and texture features into a comprehensive

optical feature set. To assess the value of multi-sensor fusion, an All S1+S2 configuration was created by integrating the complete S1 and S2 handcrafted feature stacks.

The third group evaluated foundation-model representations through three embedding-based predictor sets: AEF Embeddings, derived from the AlphaEarth Foundation model; TESSERA Embeddings; and AEF + TESSERA, which concatenated both embedding spaces into a unified latent representation. The combined remote-sensing layers were sampled at plot coordinates using a circular buffer with a radius of 17.84 m, corresponding to the field plot footprint. Mean values within each buffer were extracted and used as predictor variables for subsequent modeling analyses.

Table 1. Predictor sets used for model development and comparison. S1 refers to Sentinel-1, S2 to Sentinel-2, NDI to normalized difference index, EVI to enhanced vegetation index, RaoQ to Rao's Quadratic Entropy, and AEF to AlphaEarth Foundation.

Group	Predictor set	Description	No. features
S1	S1 Backscatter	VV and VH backscatter coefficients (ascending and descending passes)	4
S1	S1 Backscatter + NDI	S1 Backscatter plus radar-derived NDI	6
S1	S1 Textures	GLCM texture metrics (contrast, dissimilarity, entropy, homogeneity) derived from S1 imagery	4
S1	S1 Backscatter + NDI + Textures	Complete S1 feature stack	10
S2	S2 Spectral	Multispectral S2 bands (B2–B8A, B11, B12)	10
S2	S2 Spectral + EVI + RaoQ	Spectral bands plus EVI and RaoQ	13
S2	EVI Textures	GLCM texture metrics derived from multi-temporal EVI imagery	4
S2	S2 Full	Complete S2 feature stack including spectral bands, EVI, RaoQ, and texture metrics	17
Multi-sensor	All S1+S2	Combined S1 and S2 handcrafted feature stacks	27
Foundation models	AEF Embeddings	64-dimensional AlphaEarth embeddings	64
Foundation models	TESSERA Embeddings	128-dimensional TESSERA embeddings	128
Foundation models	AEF + TESSERA	Combined AlphaEarth and TESSERA embedding spaces	192

2.7. Deep Neural Network (DNN) Modeling

For each response variable, a separate feed-forward DNN was trained using Keras Sequential API with the architecture Normalization → Dense (64, ReLU) → Dense (64, ReLU) → Dense (1) (Fig. 3). The Normalization layer was fitted on the training data of each cross-validation fold only to avoid information leakage. Within each training fold, 10% of the samples were held out as a validation subset for early stopping and learning-rate scheduling. Models were optimized with RMSprop under a mean absolute error (MAE) loss, which is less sensitive to outliers, using a batch size of 256 for up to 100 epochs. Early stopping (patience = 20, restoring the best weights) and learning-rate

reduction on plateau (factor 0.5, patience = 10, minimum learning rate = 1×10^{-6}) were applied. Missing predictors were imputed by the training-split median within each fold.

DNNs were selected as the modeling framework because the predictor sets included high-dimensional foundation-model embeddings (64 dimensions for AEF and 128 dimensions for TESSERA) that were designed to encode complex, distributed, and potentially non-linear relationships. DNNs are well suited to modeling interactions among latent embedding dimensions and therefore provide a natural downstream predictor for evaluating foundation-model representations. Importantly, the objective of this study was not to compare machine-learning algorithms, but rather to assess the relative value of foundation-model embeddings and conventional handcrafted remote-sensing features for forest diversity mapping. To ensure a fair comparison, all predictor sets were evaluated using the same DNN architecture and training procedure. This unified framework minimizes the influence of algorithm-specific effects and allows differences in predictive performance to be attributed primarily to the information content of the feature representations themselves.

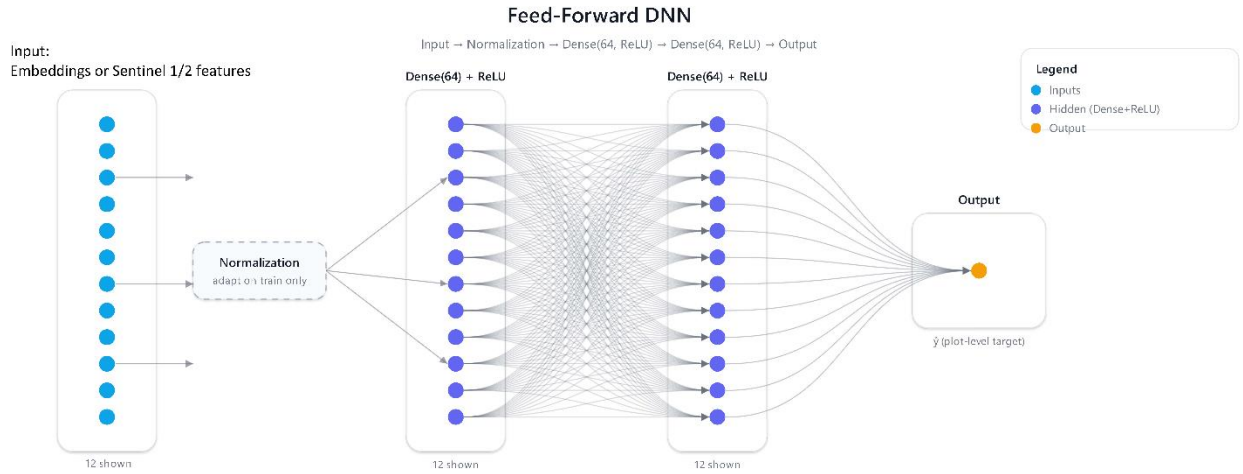

Fig. 3. Feed-forward deep neural network (DNN) architecture used to predict Shannon diversity (H′), species richness, and diameter at breast height (DBH) standard deviation from the twelve predictor sets.

2.8. Model Evaluation and Interpretation

A core risk in ecological mapping is over-optimistic accuracy when spatial dependence is ignored. Best practice, therefore, mandates blocked or buffered spatial cross-validation at spatial scales matching the range of autocorrelation (Roberts et al., 2017; Valavi et al., 2019). Methodological work shows that random cross-validation can inflate performance, whereas spatially separated folds (e.g., using blockCV) yield more realistic estimates (Valavi et al., 2019).

To reduce optimistic bias arising from spatial autocorrelation, model performance was evaluated using spatial cross-validation. The Hyrcanian forest belt was partitioned into four geographically distinct management-zone blocks (Fig. 1). In each fold, one block was withheld for testing while models were trained on the remaining three blocks, yielding a 4-fold spatial cross-validation framework. To reduce stochastic variability associated with neural-network

parameter initialization, each fold was repeated 10 times using different random seeds. The median of performance metrics was calculated across folds and repetitions. The selected block structure was designed to maximize geographic separation among training and testing data while maintaining ecologically meaningful regional partitions.

For each spatial fold, the neural network was trained ten times with different random initializations to stabilize the performance estimates. Out-of-fold metrics were reported as median ± standard deviation across all folds and repeats: coefficient of determination (R^2), root mean squared error (RMSE), and MAE (Eqs. 1–3). To interpret predictors, permutation importance was computed on each held-out fold as the increase in MAE induced by randomly permuting a feature, and permutation importances were aggregated as mean ± standard deviation across folds and repeats. Diagnostic plots included prediction-versus-observation scatterplots with a 1:1 line compiled from out-of-fold predictions and bar charts of permutation importance with error bars.

Eq. (4) $$R^2 = 1 - \frac{\sum(y_i - \widehat{y_i})^2}{\sum(y_i - (\overline{y_i})^2}$$

Eq. (5) $$RMSE = \sqrt{\frac{1}{n}\sum(y_i - \widehat{y_i})^2}$$

Eq. (6) $$ME = \frac{1}{n}\sum \widehat{y_i} - y_i$$

SAR and optical preprocessing were implemented in Google Earth Engine; GIS data handling, projection checks, vector cleaning, mask delineation, and cartographic preparation were performed in QGIS 3.4. Modelling and evaluation were conducted in Python using TensorFlow/Keras, scikit-learn, NumPy, and pandas.

3. Results

3.1. Performance of feed-forward deep neural networks (DNNs)

Modeling results indicate that embedding-based feature sets generally achieved higher median R^2 values than handcrafted Sentinel-derived predictors (Table 2) and that AEF consistently had an advantage over TESSERA. The predictive performance of both embedding architectures and standard remote sensing stacks was highest for structural diversity, followed by moderate performance for Shannon diversity and species richness.

A clear hierarchy emerged among the handcrafted predictor sets. Across all three diversity indicators, S2 spectral and texture features consistently outperformed S1 radar-based predictors. In contrast, S1-derived backscatter, NDI, and texture metrics alone exhibited very limited predictive power, with several S1 configurations yielding near-zero explanatory capacity. Moreover, combining the complete S1 and S2 feature stacks ("All S1+S2") resulted in only marginal improvements relative to the best S2-only configurations and did not alter the overall ranking of the models.

In the context of Shannon diversity, embedding-based configurations maintained their superior predictive rank. The combined AEF + TESSERA feature set led the results with a median R^2 of 0.50, closely followed by individual AEF embeddings (median R^2= 0.48) and TESSERA embeddings (median R^2= 0.46). The strongest non-embedding alternative was the combined "All S1+S2" feature stack, which yielded a median R^2 of 0.37. Notably, the integration

of EVI and Rao's Q metrics into the S2 spectral data did not enhance performance, with the "S2 Spectral + EVI + RaoQ" stack underperforming the core "S2 Spectral" baseline (R^2 0.35 vs. 0.37, respectively).

For species richness, the combined AEF + TESSERA embeddings achieved the highest predictive accuracy, yielding a median R^2 of 0.46. Among the individual foundation models, AEF embeddings (R^2 = 0.41) slightly outperformed TESSERA embeddings (R^2 = 0.40). The best handcrafted alternative was the "S2 Spectral" configuration, which achieved a median R^2 of 0.35 and an RMSE of 0.82, while the more complex "S2 Spectral + EVI + RaoQ + EVI Textures" stack reached a median R^2 of 0.32.

For structural diversity, the AEF embeddings achieved the highest overall predictive accuracy with a median R^2 of 0.62, an RMSE of 3.34, and an MAE of 2.71. This outperformed the combined AEF + TESSERA stack (median R^2 = 0.58, RMSE = 3.43) and marked a substantial improvement over the strongest handcrafted baseline, "S2 Spectral + EVI + RaoQ + EVI Textures" (median R^2 = 0.46, RMSE = 3.95). The "All S1+S2 Features" stack performed similarly (R^2 = 0.45), whereas TESSERA embeddings alone achieved a median R^2 of 0.46. In contrast to the embedding-based models and S2 configurations, S1 baseline sets exhibited limited predictive capacity; the "S1 Textures" band set yielded the lowest performance with a median R^2 of only 0.02.

Across all three target variables, standard S2 spectral and texture features consistently outperformed S1 backscatter and texture configurations. Furthermore, the standard deviation across validation folds remained low for all evaluated models, with R^2 standard deviations generally ranging between 0.01 and 0.06, indicating stable model behavior and robust ranking of feature sets under the spatial cross-validation framework.

Table 2. Performance of feed-forward Deep Neural Networks (DNNs) by target and predictor band set (median and fold-to-fold standard deviation under spatial cross-validation). In **bold**, the best results by target variable, and underlined the second-best. S1 refers to Sentinel-1, S2 to Sentinel-2, NDI to normalized difference index, EVI to Enhanced Vegetation Index, RaoQ to Rao's Quadratic Entropy, AEF to AlphaEarth Foundation, n feat to the number of features, RMSE to Root Mean Squared Error, and MAE to Mean Absolute Error.

			Median			Standard deviation		
target	Band set	n feat	R^2	RMSE	MAE	R^2	RMSE	MAE
Shannon H′	S1 Backscatter	4×23	0.15	0.26	0.20	0.03	0.01	0.01
	S1 Backscatter + NDI	6×23	0.12	0.26	0.20	0.03	0.01	0.01
	S1 Textures	4×23	0.00	0.28	0.21	0.02	0.02	0.02
	S1 Backscatter + NDI + Textures	10×23	0.09	0.26	0.20	0.04	0.01	0.01
	S2 Spectral	10×23	0.37	0.22	0.17	0.06	0.01	0.01
	S2 Spectral + EVI + RaoQ	13×23	0.35	0.22	0.17	0.05	0.01	0.01
	EVI Textures	4×23	0.26	0.24	0.18	0.02	0.02	0.02
	S2 Full	17×23	0.36	0.22	0.17	0.04	0.01	0.01
	All S1+S2	(10+17)×23	0.37	0.22	0.17	0.05	0.01	0.01
	AEF	64	0.48	0.21	0.17	0.05	0.01	0.01
	TESSERA	128	0.46	0.21	0.17	0.06	0.01	0.01

	AEF + TESSERA	**64+128**	**0.50**	**0.20**	**0.16**	**0.05**	**0.01**	**0.01**
Species richness	S1 Backscatter	4×23	0.05	0.97	0.77	0.05	0.03	0.03
	S1 Backscatter + NDI	6×23	0.14	0.94	0.76	0.04	0.04	0.03
	S1 Textures	4×23	0.02	1.00	0.82	0.05	0.04	0.04
	S1 Backscatter + NDI + Textures	10×23	0.10	0.96	0.77	0.05	0.03	0.03
	S2 Spectral	10×23	0.35	0.82	0.66	0.02	0.03	0.02
	S2 Spectral + EVI + RaoQ	13×23	0.31	0.84	0.68	0.02	0.03	0.02
	EVI Textures	4×23	0.18	0.93	0.73	0.03	0.04	0.03
	S2 Full	17×23	0.32	0.83	0.67	0.01	0.03	0.02
	All S1+S2	(10+17)×23	0.31	0.84	0.68	0.02	0.03	0.03
	AEF	64	0.41	0.75	0.60	0.03	0.03	0.02
	TESSERA	128	0.40	0.79	0.63	0.04	0.03	0.02
	AEF + TESSERA	**64+128**	**0.46**	**0.75**	**0.60**	**0.03**	**0.03**	**0.02**
DBH std (cm)	S1 Backscatter	4×23	0.11	5.14	4.13	0.04	0.23	0.23
	S1 Backscatter + NDI	6×23	0.12	5.02	4.13	0.03	0.13	0.15
	S1 Textures	4×23	0.02	5.30	4.34	0.03	0.22	0.21
	S1 Backscatter + NDI + Textures	10×23	0.11	5.06	4.15	0.04	0.13	0.15
	S2 Spectral	10×23	0.37	4.27	3.55	0.06	0.19	0.12
	S2 Spectral + EVI + RaoQ	13×23	0.41	4.15	3.37	0.05	0.21	0.16
	EVI Textures	4×23	0.35	4.34	3.41	0.04	0.20	0.17
	S2 Full	17×23	0.46	3.95	3.21	0.03	0.13	0.14
	All S1+S2	(10+17)×23	0.45	4.02	3.22	0.02	0.11	0.11
	AEF	**64**	**0.62**	**3.34**	**2.71**	**0.05**	**0.14**	**0.12**
	TESSERA	128	0.46	3.98	3.12	0.04	0.14	0.18
	AEF + TESSERA	64+128	0.58	3.43	2.73	0.04	0.17	0.15

The scatter plots in Fig. 4 illustrate the relationship between observed and predicted values for the three target ecological variables, comparing the performance of AEF embeddings, TESSERA embeddings, and the "All S1+S2 Features" baseline. For Shannon diversity, the AEF embeddings model produces a relatively tight cloud of points that tracks the 1:1 line more effectively than the other models, demonstrating robust calibration across the entire diversity range. In contrast, while the "All S1+S2 Features" model captures the general positive trend, it displays a flatter distribution characterized by a pronounced tendency to over-predict at low diversity levels and under-predict at high diversity levels. TESSERA embeddings show intermediate performance, matching the low MAE of the AEF model but displaying slightly more dispersion.

Regarding species richness, all models exhibit distinct results. The AEF embeddings model aligns closest to the 1:1 line, particularly across the core range of 2 to 5 species. However, it still exhibits minor regression to the mean, under-predicting the highest richness values. The "All S1+S2 Features" baseline exhibits a more pronounced compression bias, with its trend line flattening considerably at the extremes and failing to capture stands with low or high species counts. TESSERA embeddings capture this target moderately well, though with a slightly wider spread than AEF.

Differences among feature sets were largest for structural diversity. The AEF embeddings model showed the highest explanatory performance among evaluated configurations, with its smoothed trend line tightly tracking the 1:1 line across the entire 5 to 30 cm range and minimizing prediction error at both extremes. TESSERA embeddings and the "All S1+S2 Features" baseline yield comparable overall explanatory power. However, the "All S1+S2 Features" model suffers from a higher RMSE and exhibits greater overall dispersion, confirming that while handcrafted features can track the broader structural trend, they show greater dispersion and lower calibration for fine-scale structural variability than the AEF embeddings (Fig. 4).

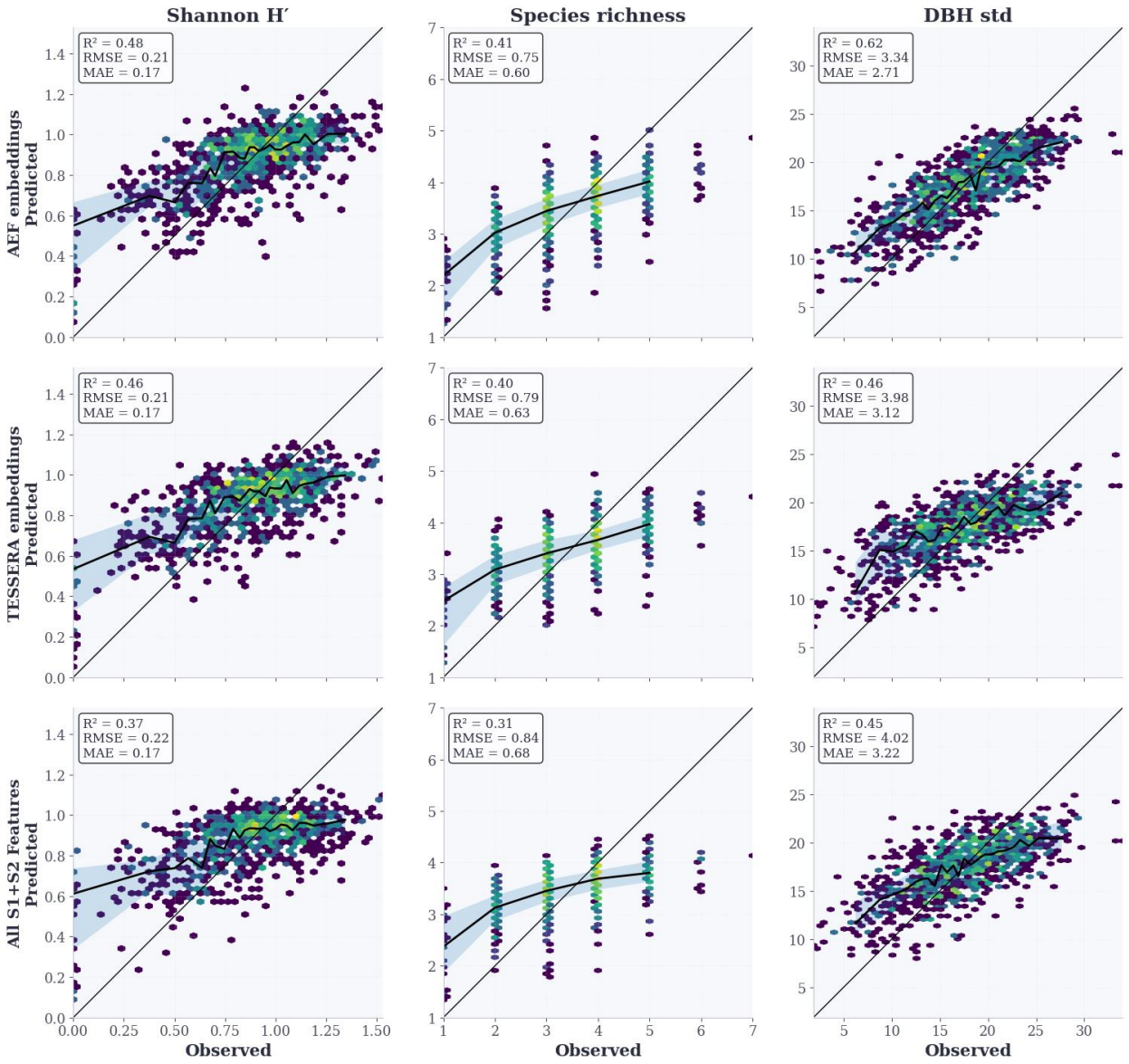

Fig. 4. Prediction vs. Observation (color = observation density in hexagonal bins, log-scaled; diagonal line = 1:1 perfect agreement; solid curve = running median; shaded band = IQR). S1 refers to Sentinel-1, S2 to Sentinel-2, AEF to AlphaEarth Foundation, and std to standard deviation.

3.2. Feature importance

The feature-importance profiles reveal distinct patterns between handcrafted Sentinel predictors and foundation-model embeddings (Fig. 5), although these results should be interpreted cautiously because permutation importance can underestimate the contribution of correlated variables by distributing predictive information across multiple features. Consequently, the rankings identify influential predictors but do not necessarily imply that only the highest-ranked features are required for accurate prediction.

Across all feature sets, permutation-importance values declined gradually from the highest- to lower-ranked predictors, with no evidence of a single feature dominating model performance (Fig. 5). This pattern indicates that predictive accuracy depends on the combined contribution of multiple variables rather than a small number of dominant predictors. However, notable differences were observed in the magnitude of feature importance among the three predictor sets. The highest-ranked AEF and TESSERA dimensions consistently exhibited larger permutation-importance values than the highest-ranked S1/S2 variables across all response variables. This suggests that individual embedding channels contain more unique predictive information, whereas the predictive signal in the handcrafted Sentinel feature set is distributed across a larger number of correlated spectral, temporal, and texture variables. As a result, permuting any single Sentinel predictor produced only a modest reduction in model performance.

The relatively gradual decline in importance values among the top-ranked embedding dimensions further indicates that predictive information is distributed across multiple latent channels rather than concentrated within a few dominant features. Together, these results suggest that foundation-model embeddings provide compact representations in which individual dimensions capture comparatively strong and complementary ecological information, whereas conventional Sentinel-derived predictors rely on a larger set of partially redundant variables to achieve comparable predictive performance.

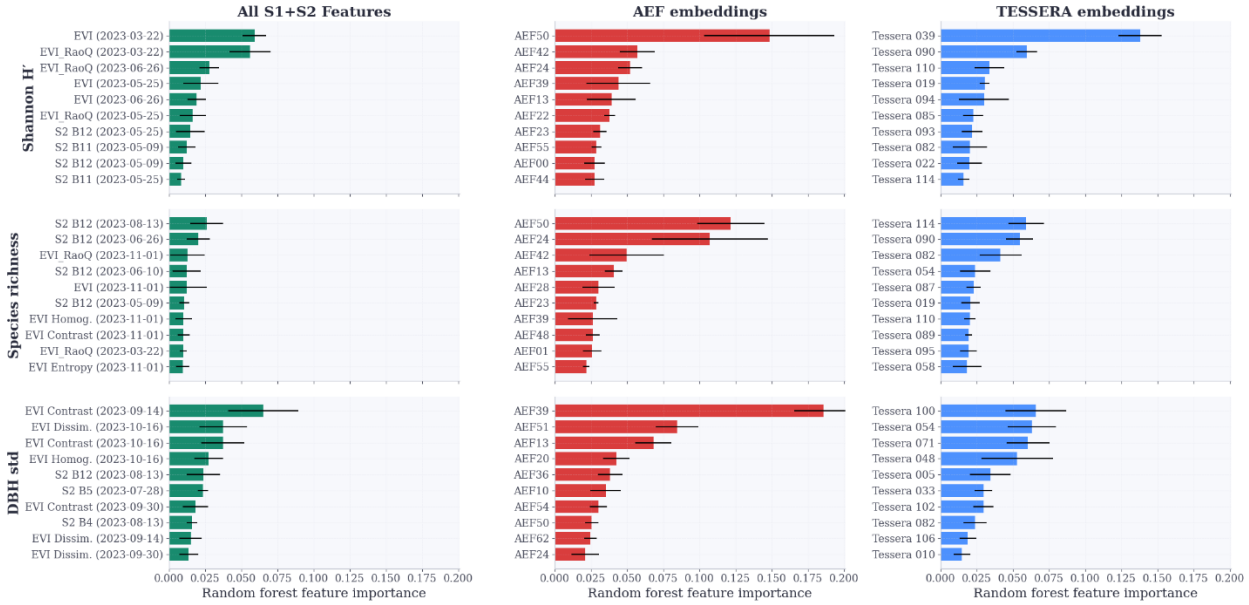

Fig. 5. Permutation feature importance (ΔMAE) for deep neural network (DNN) models by target and predictor family.

3.3. UMAP Analysis of Predictor Representations

The UMAP projections derived from the S1+S2, AEF, and TESSERA feature sets reveal broadly continuous manifolds with substantial mixing of plots across the full range of Shannon diversity (H′), species richness, and DBH standard deviation (Fig. 6). No clear, well-defined clusters corresponding to taxonomic diversity levels are evident, as plots with low and high Shannon H′ values and species richness are distributed throughout the embedding space. Nevertheless, plots exhibiting the lowest diversity levels tend to occur more frequently along the outer margins of the manifolds, particularly in localized peripheral regions, suggesting that highly simplified forest stands possess spectral and structural characteristics that differ from those of more heterogeneous forests.

Among the evaluated response variables, DBH standard deviation exhibits the most discernible spatial organization within the embeddings. Although the gradient remains diffuse, plots with higher structural heterogeneity are more frequently concentrated in specific regions of the latent space, whereas plots with low DBH variability are more common near the edges of the manifolds. This pattern is most apparent in the AEF representation and, to a lesser extent, in TESSERA and the conventional S1+S2 feature space. However, the substantial overlap among color classes indicates that structural diversity is only partially encoded in the learned representations.

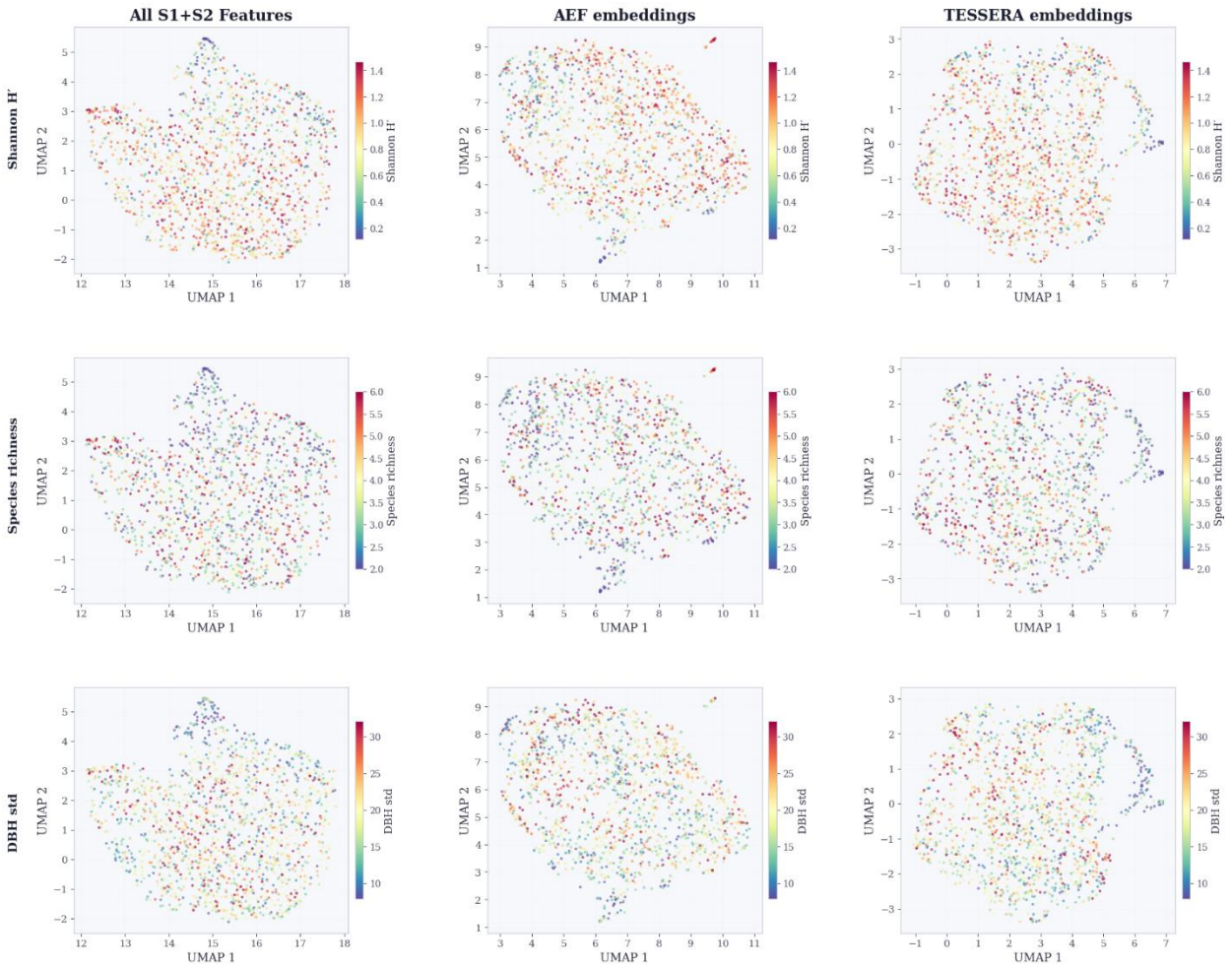

Fig. 6. Two-dimensional Uniform Manifold Approximation and Projection (UMAP) representations of the predictor spaces derived from the handcrafted Sentinel-1/Sentinel-2 feature stack (S1+S2), AlphaEarth Foundation (AEF) embeddings, and TESSERA embeddings. Points are colored according to Shannon diversity (top row), species richness (middle row), and structural diversity expressed as the standard deviation of DBH (bottom row)

3.4. Exploring the effect of tree size and density on modeling

Error stratification across Quadratic Mean Diameter (QMD) classes indicates that prediction uncertainty remains broadly stable across the tree-size gradient for all modeling frameworks (Fig. 7). For Shannon diversity, median absolute residuals show only modest variation among QMD classes, with slightly elevated errors occurring in some intermediate diameter ranges. Species richness exhibits a similarly weak dependence on stand diameter, although several mid-sized and larger diameter classes display somewhat wider interquartile ranges (IQRs), indicating increased variability in prediction accuracy. The clearest differences are observed for structural diversity (DBH std), where residuals remain consistently higher than those observed for the taxonomic diversity metrics. Nevertheless, no systematic increase in error is evident toward larger diameter classes. Across most QMD strata, the AEF and

TESSERA embedding models generally produce slightly lower median residuals and somewhat narrower error distributions than the handcrafted S1+S2 feature model, particularly for Shannon diversity and DBH variability. Overall, these results suggest that prediction performance is relatively robust across the structural development gradient of the studied forests, with foundation-model embeddings providing modest but consistent improvements in error stability compared with conventional handcrafted remote-sensing features.

A similar pattern emerges when residuals are stratified by stem density (trees ha^{-1}) (Fig. 8). For Shannon diversity and species richness, median absolute residuals remain relatively stable across the density gradient, with only minor fluctuations among density classes and no evidence of a systematic deterioration in prediction accuracy in denser stands. Although some intermediate and high-density classes exhibit slightly wider IQRs, indicating increased variability in individual predictions, the overall magnitude of errors remains comparable across the full range of stem densities. For structural diversity (DBH std), residuals are consistently larger than those observed for the taxonomic diversity metrics, but again show little sensitivity to changes in stand density. Across nearly all density classes, the AEF and TESSERA embedding models tend to exhibit lower median residuals and more compact error distributions than the handcrafted S1+S2 feature model, suggesting greater robustness to variation in stand structure. Collectively, these findings indicate that prediction performance is largely insensitive to both tree size and stem density gradients. At the same time, foundation-model embeddings provide modest but consistent gains in error stability across a broad spectrum of forest structural conditions.

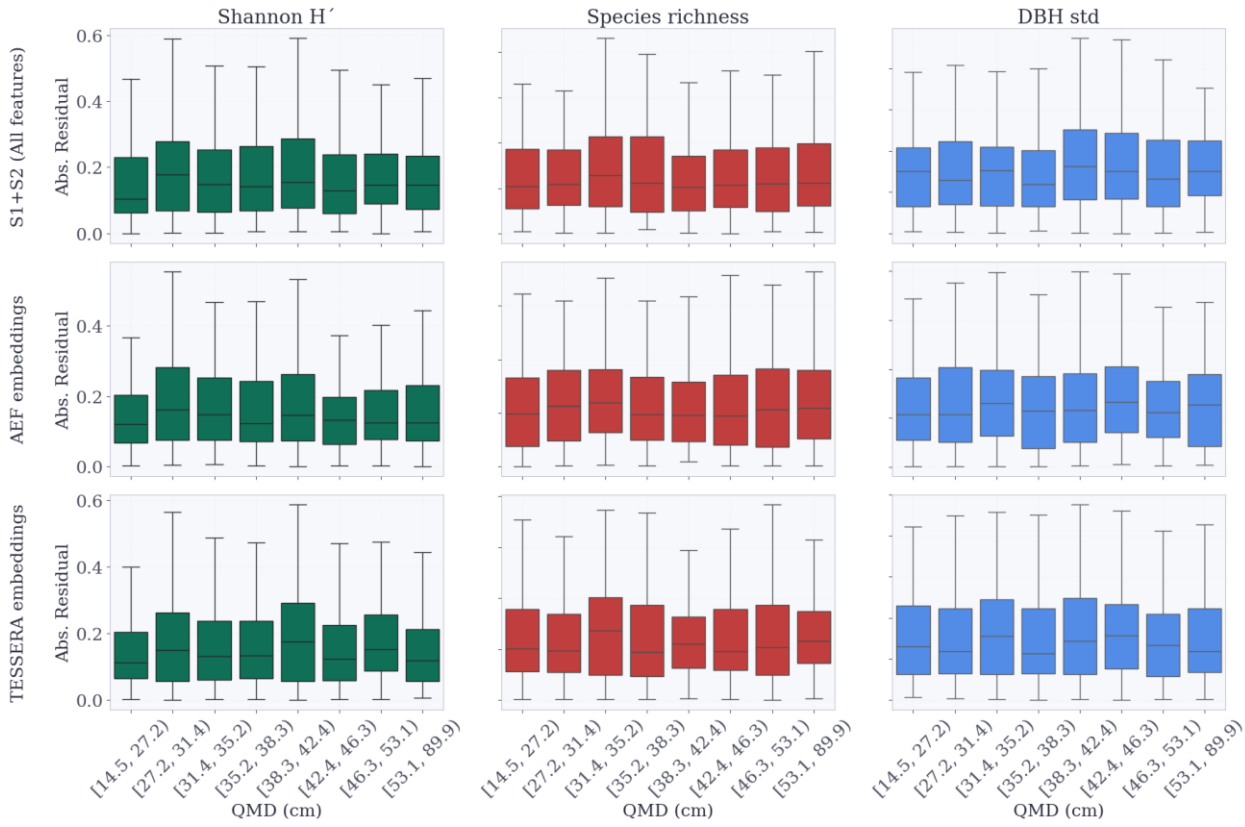

Fig. 7. Error stratification across stand structure for DNN models (absolute residuals grouped by QMD). QMD (x-axis): Quadratic Mean Diameter of trees in the plot.

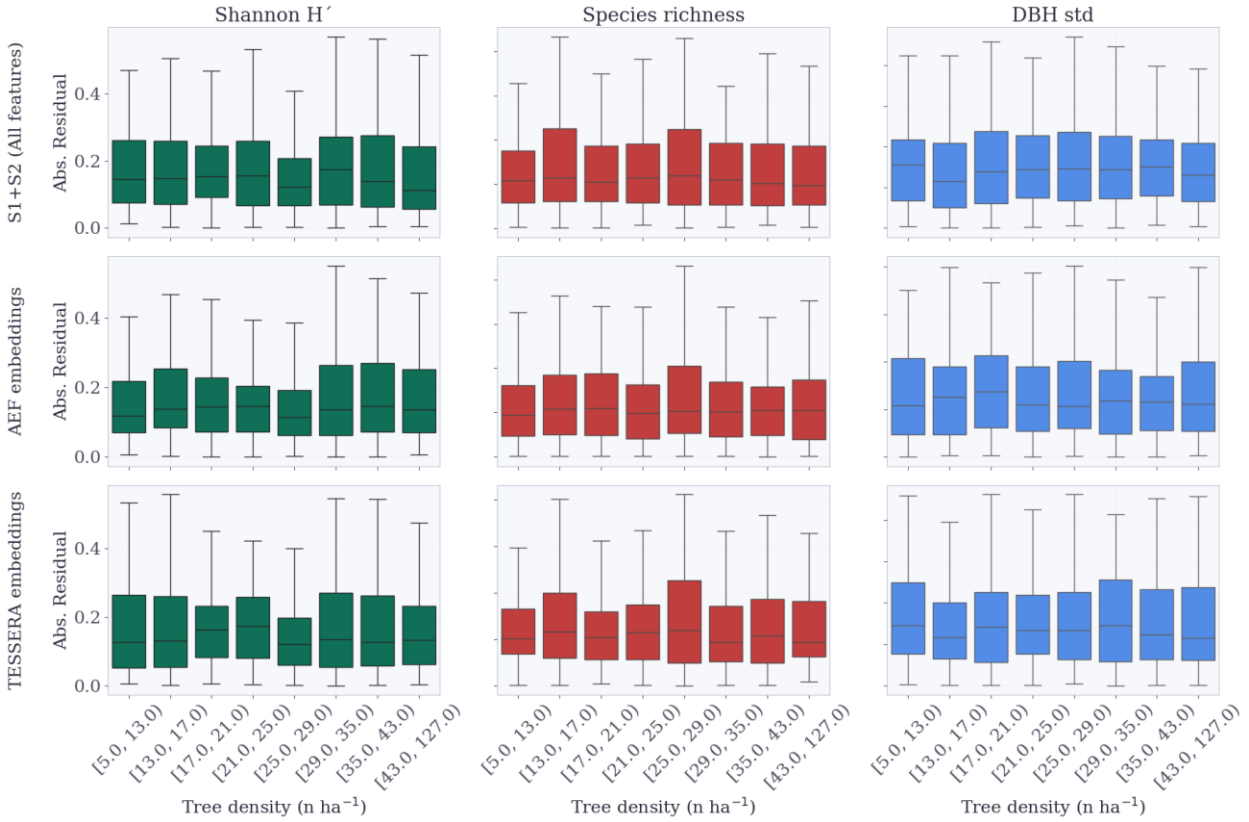

Fig. 8. Error stratification across stand structure for DNN models (absolute residuals grouped by tree density).

3.5. Wall-to-wall maps

Wall-to-wall predictions of three forest-diversity indicators across the Hyrcanian forest belt were generated using the best-performing AEF embedding models (Fig. 9). Fig. 9A shows taxonomic diversity measured by Shannon's diversity index, while Fig. 9B and Fig. 9C represent species richness (number of tree species per plot) and the standard deviation of diameter at breast height, respectively.

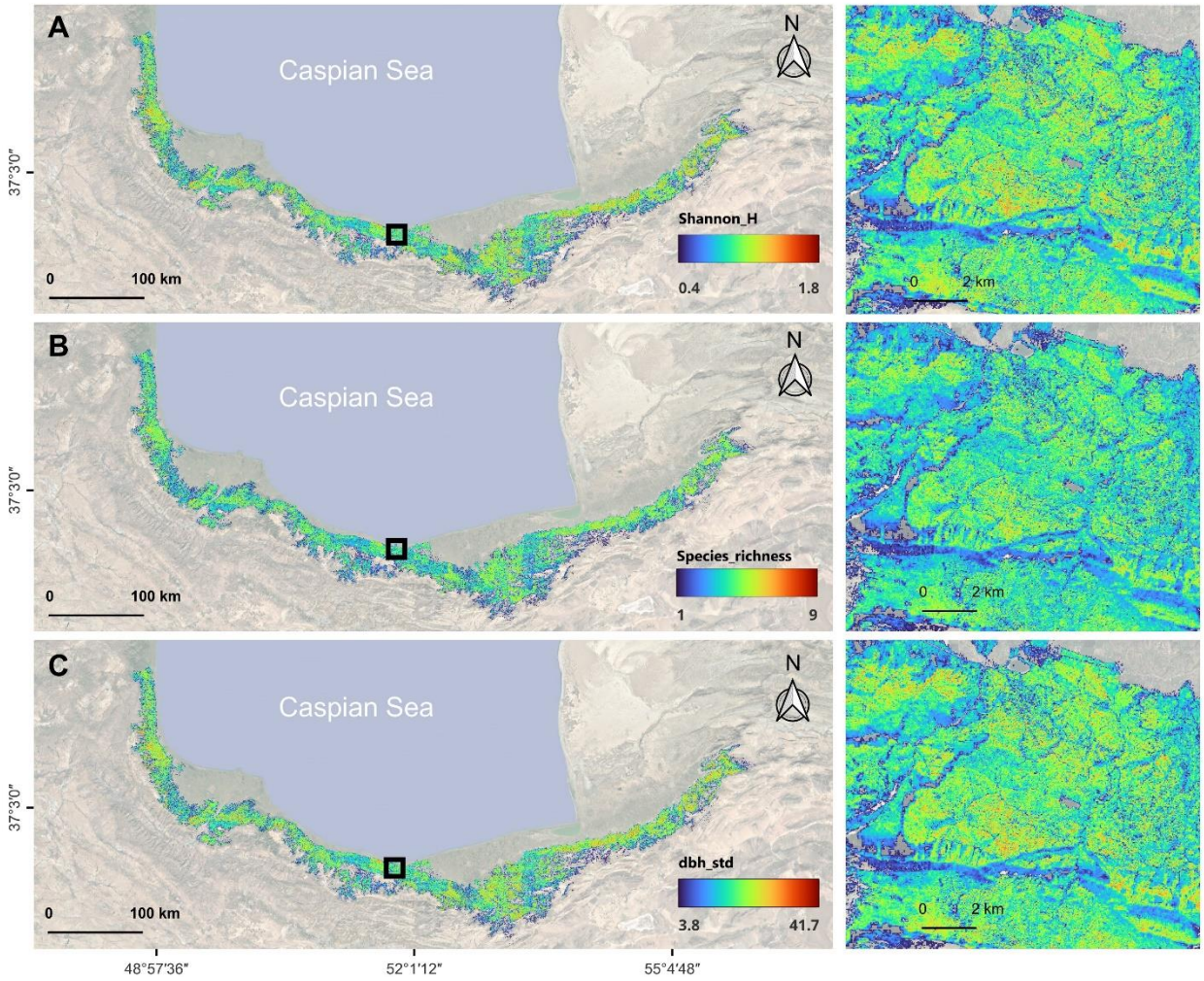

Fig. 9. Predicted spatial patterns of structural and taxonomic forest diversity across the Hyrcanian forests derived from AlphaEarth Foundation (AEF) embeddings. Maps are masked to the official Hyrcanian Forest Boundary.

4. Discussion

4.1. Embeddings vs. handcrafted features

A consistent performance hierarchy was observed across all three target ecological variables, with foundation-model embeddings (in particular AEF) outperforming the sensor-specific stacks: AEF > TESSERA > S2 Full >> S1. Amongst the isolated single-sensor configurations, S2 spectral was almost on par with the embedding-based models, whereas S1-backscatter was largely useless and did not add value when combined with the S2 stack. Combining the two embeddings did not yield performance gains over using AEF alone.

The distinct advantage of foundation models was most apparent in characterizing structural diversity. While the strongest handcrafted predictor configuration (S2 Full) achieved a median R^2 of 0.46 (RMSE = 3.95), embedding-based representations substantially improved predictive performance. The AEF model achieved the highest accuracy

among all evaluated predictor sets, with a median R^2 of 0.62 and RMSE of 3.34, representing a marked improvement over handcrafted Sentinel-derived features. The combined AEF + TESSERA model also performed strongly (R^2 = 0.58, RMSE = 3.43), whereas TESSERA alone performed comparably to S2 Full (R^2 = 0.46, RMSE = 3.98). These findings demonstrate the particular value of foundation-model embeddings for representing forest structural variability.

These performance differences suggest that the embeddings may better capture structural and canopy-related information not fully represented by the handcrafted predictors. These findings align with recent literature demonstrating that deep, self-supervised representations effectively generalize across downstream ecological tasks by reusing complex spatio-temporal features (Lu et al., 2025; Xiao et al., 2025). However, the comparison should not be interpreted as a strictly controlled architectural comparison because the pretrained AEF embedding products incorporate auxiliary information sources (e.g., GEDI, terrain, and climate variables) that were not explicitly represented within the handcrafted Sentinel-based predictors. Similarly, TESSERA is based solely on S1 and S2 data, and no attempts were made to add textural features.

While traditional handcrafted feature stacks offer interpretability, they dilute predictive signals across dozens of collinear spectral indices and spatial texture layers. Furthermore, their performance is highly sensitive to subjective analytical choices, such as the timing of the cloud-free compositing window, local moving-window texture dimensions, and phenological matching. Conversely, the AEF embedding model displayed better-calibrated alignment with the 1:1 line across all targets. Crucially, because these models were evaluated using a strict, spatially explicit block cross-validation, these performance gains reflect genuine macro-ecological modeling capacity; traditional random cross-validation would potentially have obscured these architectural differences by overstating the performance of handcrafted features through spatial autocorrelation over-fitting (Roberts et al., 2017; Valavi et al., 2019).

Ultimately, foundation-model embeddings deliver both higher absolute predictive accuracy and superior error stability across diverse stand conditions without any further model fine-tuning, by simply adding a prediction head. The most substantial operational gains are concentrated in small-diameter cohorts and highly dense canopies, where traditional handcrafted features incur pronounced error inflation. This supports growing evidence that deep remote sensing representations successfully encode subtle, sub-pixel canopy variations that are important for monitoring heterogeneous, multi-layered forest ecosystems (Hoffmann et al., 2022).

Despite their predictive advantages, foundation-model embeddings remain substantially less interpretable than spectral indices or texture metrics. The latent dimensions identified as important in the downstream models do not correspond to directly observable ecological variables, and their functional meaning cannot be inferred solely from permutation importance rankings. Consequently, mechanistic interpretations regarding canopy structure, moisture dynamics, or phenological sensitivity should be considered provisional. Future work should combine embedding attribution analysis, latent-space probing, and controlled ablation experiments to better understand the ecological information represented within these pretrained feature spaces.

4.2. Comparison with prior Hyrcanian studies

The predictive accuracies and spatial stability achieved in this study are broadly higher and more robust than those reported in historical Hyrcanian forest research, which traditionally leaned on handcrafted spectral features and conventional machine learning architectures. Early baseline work utilizing Landsat ETM+ data attempted to relate plot-level species richness, Shannon diversity, or Simpson indices to raw spectral bands and simple mathematical transformations; while these models achieved moderate local fits, they exhibited pronounced sensitivity to index selection, sensor degradation, and spatial scale (Hashemi et al., 2012; Mohammadi et al., 2020; Mohammadi and Shataee, 2010). Subsequent efforts integrated very-high-resolution (VHR) commercial tasking sensors (e.g., Pléiades, GeoEye) with advanced non-parametric classifiers such as GAM, MARS, SVM, and RF. Although these VHR workflows improved local biodiversity mapping within isolated experimental districts, their model transferability across different bioclimatic zones remained highly uncertain and cost-prohibitive (Akbari and Kalbi, 2019a, 2019b, 2016). Multi-modal optical-SAR fusion studies in the region demonstrated that incorporating terrain topography yielded performance gains in steep, dissected terrain, though errors varied significantly by slope class and aspect (Attarchi & Gloaguen, 2013, 2018). Furthermore, cross-sensor evaluations for local species classification repeatedly highlighted the importance of NIR and red-edge bands, yet yielded only incremental, sensor-to-sensor improvements (Soleimannejad et al., 2019).

More recent S2 initiatives utilizing continuous spectral diversity metrics and spatial textures still reported modest R^2 values at the plot scale (Ghaisaryan et al., 2023), while specialized frameworks like the PaRaVis toolbox emphasized multi-index, multi-temporal RaoQ for unsupervised α- and β-diversity mapping rather than explicit, supervised regression modeling (Fathi et al., 2024). Against this backdrop, the present embedding-based frameworks, evaluated under a spatially structured cross-validation design, produced significantly stronger calibration curves and superior explanatory power across all targets. This confirms that self-supervised representation learning captures latent canopy signals that traditional index- and texture-only stacks leave entirely unutilized.

For structural diversity mapping, prior Hyrcanian literature illustrates both the promise of advanced active sensors and their inherent operational limitations. For instance, space-borne polarization coherence tomography derived from TanDEM-X radar data explained only a small fraction of local DBH variation and stem density, even after rigorous geometric calibration (Poorazimy et al., 2023). While fusion of airborne laser scanning and digital aerial photogrammetry significantly improved a suite of structural diversity indices, these workflows rely on costly, localized airborne campaigns and lack the wall-to-wall, continuous coverage required for regional conservation planning (Mohammadi et al., 2020).

Regional spaceborne LiDAR modeling utilizing GEDI footprints has advanced the estimation of basal area, stand volume, and stem density, yet its continuous interpolation hinges entirely on satellite orbit constraints, cloud cover gaps, and sparse sampling patterns (Sohrabi and Akhavan, 2026). In contrast, the foundation-model embeddings evaluated in this study provide spatially continuous 10 m representations derived from large-scale Earth observation data. When coupled with a DNN, these embeddings captured plot-scale DBH variability substantially better than handcrafted Sentinel-derived predictors. The AEF model achieved the highest performance ($R^2 = 0.62$, RMSE = 3.34), compared with the strongest handcrafted configuration, All S1+S2 features ($R^2 = 0.46$, RMSE = 3.95). This performance advantage suggests that foundation-model embeddings encode information relevant to forest structural

heterogeneity that is not fully captured by conventional spectral, index-based, and texture-based predictors. Although the internal representation learned by these models is not directly interpretable, the results indicate that embedding-based approaches provide a more effective feature space for modeling structural diversity across heterogeneous temperate forests.

Methodological validation choices also explain the stark performance discrepancies between this work and historical baselines. Many earlier Hyrcanian studies relied on random or only partially restricted cross-validation designs, a flaw that inadvertently permits data leakage and inflates accuracy metrics in highly autocorrelated forest environments (Ghaisaryan et al., 2023; Mohammadi et al., 2011; Mohammadi and Shataee, 2010). Here, the implementation of spatially explicit cross-validation enforced a strict geographic separation between training and validation folds, ensuring that the reported errors reflect genuine, out-of-sample ecological generalization. Additionally, previous regional studies were frequently confined to small-area or single-district inventories comprising only tens to a few hundred plots, which restricted model capacity.

By leveraging a comprehensive network of plots spanning the environmental and structural gradients of the Hyrcanian forest belt, this study provides a rigorous benchmark comparison between foundation-model embeddings and handcrafted remote-sensing predictor sets. Although performance improvements varied among response variables, embedding-based representations consistently outperformed conventional Sentinel-derived features. The gains were particularly evident for taxonomic diversity, where the best embedding models increased predictive performance from R^2 values of approximately 0.35 for Shannon diversity and 0.35 for species richness using the strongest handcrafted Sentinel-2 predictors to 0.50 and 0.46, respectively. Structural diversity exhibited the largest improvement, with AEF increasing R^2 from 0.46 (All S2+S2 Features) to 0.62. These findings suggest that foundation-model embeddings capture ecological information relevant to both compositional and structural variation that is only partially represented by handcrafted spectral, index-based, and texture-derived predictors. While Sentinel-2 variables alone provided reasonably strong baselines, particularly for Shannon diversity and species richness, embedding-based representations offered a more informative feature space for characterizing forest heterogeneity across the complex environmental gradients of the Hyrcanian forests.

4.3. Structural diversity

Results for structural diversity revealed clear architectural and data-driven performance. While traditional inputs, such as isolated S1, S2, or independent texture bandsets, captured the broader structural trajectory, they exhibited wider error dispersion and a pronounced compression bias. In contrast, the embedding models demonstrated a highly calibrated, positive linear slope and significantly tighter residuals across the structural space. This indicates that self-supervised embeddings carry rich, multi-dimensional structural signals that simple indices and spatial textures fail to adequately capture (Mohammadi and Shataee, 2010).

A notable performance gap was observed between the two foundation-model frameworks. For structural diversity (DBH std), AEF achieved a median R^2 of 0.62, substantially outperforming TESSERA ($R^2 = 0.46$) and all handcrafted predictor sets. This finding highlights that not all foundation-model embeddings provide equivalent ecological

information for downstream tasks. While the specific factors responsible for this difference cannot be determined from the present analysis, variations in model architecture, training objectives, and input data sources likely contribute to the stronger representation of forest structural heterogeneity captured by AEF. One possible explanation for this difference is the inclusion of GEDI-derived structural information within the AEF pretraining framework. By contrast, TESSERA relies primarily on multi-temporal optical and C-band SAR streams without native GEDI constraints. These active LiDAR sources appear to encode vertical canopy profiles and horizontal stand structural attributes that are completely absent from standard S1/S2 handcrafted baselines. With these complex architectural cues embedded directly within the latent feature space, the downstream DNN can effectively differentiate and separate forest plots that present identical spectral signatures but possess highly divergent structural profiles.

The limited capacity of single-date shortwave infrared (SWIR) bands and handcrafted EVI textures to resolve fine-scale DBH variation is expected under dense forest conditions. While SWIR responds strongly to canopy moisture and EVI textures reflect coarse horizontal patterning, within-stand diameter variation is an internal structural metric that is only weakly linked to surface-level spectral summaries. Where wall-to-wall data is available, LiDAR remains the premier proxy for structural characterization. However, the results presented here demonstrate an important operational development: by leveraging AEF's self-supervised latent space, downstream models appear capable of leveraging structural information associated with canopy organization even in geographical regions lacking direct, continuous LiDAR labels. This highlights a highly promising pathway for robust biodiversity and biomass monitoring across regions with sparse or fragmented LiDAR coverage (Armston et al., 2021; Schneider et al., 2020).

4.4. Taxonomic diversity

For taxonomic α-diversity indices (Shannon H' and species richness), the foundation-model embeddings consistently demonstrated superior predictive performance relative to handcrafted Sentinel-derived predictors, although the magnitude of improvement was smaller than that observed for structural diversity. The best embedding models achieved R^2 values of 0.50 for Shannon diversity and 0.46 for species richness, compared with 0.37 and 0.35, respectively, for the strongest handcrafted Sentinel-2-based predictor sets. Both AEF and TESSERA generally exhibited closer agreement with observed values and narrower residual distributions than the handcrafted alternatives, while the conventional models still provided reasonably strong predictive performance. Notably, adding Sentinel-1 variables to Sentinel-2 predictors did not improve accuracy, as the All S1+S2 model performed similarly to or slightly worse than the best Sentinel-2-only configurations ($R^2 = 0.37$ for Shannon diversity and $R^2 = 0.31$ for species richness). This pattern is consistent with previous studies showing that optical spectral information, particularly red-edge, near-infrared, and shortwave infrared wavelengths, captures much of the variation in vegetation composition and diversity, whereas Sentinel-1 backscatter often contributes limited additional information for predicting taxonomic diversity in closed-canopy forests(Immitzer et al., 2019; Misra et al., 2020; Ren et al., 2023; Yang et al., 2022).

Historically, reported biodiversity mapping accuracies in Hyrcanian forest literature utilizing combined S1 and S2 feature stacks have been moderate, fluctuating significantly based on local topographic shadows, complex overstory species mixes, and specific inventory plot designs (Akbari and Kalbi, 2019b, 2016; Mohammadi et al., 2020; Mohammadi and Shataee, 2010; Poorazimy et al., 2023). The systematic advantage of foundation-model embeddings over handcrafted feature stacks suggests that the pretrained representations capture ecologically relevant information not fully captured by conventional remote-sensing features. Because these embeddings are learned from large-scale multi-temporal observations during pretraining, they may encode complex spatial, temporal, and cross-sensor relationships that are difficult to reproduce through manual feature engineering. Nevertheless, the relative contribution of these factors remains an open question and was beyond the scope of the present study.

Although the foundation-model embeddings consistently outperformed the handcrafted feature stacks, the underlying reasons for this advantage remain unclear. The embeddings may capture information related to canopy structure, phenology, spatial context, or other environmental gradients that are only partially represented by conventional remote-sensing variables. Disentangling these contributions would require dedicated analyses beyond the scope of the present study. In practical application, standard S2 spectral stacks remain a highly reliable, computationally lightweight baseline for operational taxonomic mapping by conservation agencies. However, the foundation embeddings provide a more accurate alternative that effectively flattens systematic over- and under-prediction biases at the ecological extremes, offering a highly calibrated boost to regional biodiversity inventories.

4.5. Importance of the predictors

The permutation-importance analysis identified several influential handcrafted predictors, including SWIR bands, seasonal EVI metrics, and texture-derived variables, which are broadly consistent with previous studies highlighting the importance of canopy moisture, phenology, and vegetation heterogeneity for biodiversity mapping (Delegido et al., 2011; Fassnacht et al., 2016; Frampton et al., 2013). However, the results also highlight important limitations of conventional feature-importance analyses when applied to foundation-model embeddings.

Across all feature sets, permutation-importance values declined gradually from the highest- to lower-ranked predictors, with no evidence of a single feature dominating model performance. This pattern suggests that predictive accuracy depends on the collective contribution of multiple variables rather than a small set of dominant predictors. Nevertheless, the highest-ranked AEF and TESSERA dimensions consistently exhibited larger permutation-importance values than the highest-ranked S1/2 variables. This finding suggests that individual embedding channels contain more unique predictive information, whereas the predictive signal in the handcrafted Sentinel feature set is distributed across a larger number of correlated spectral, temporal, and texture variables. Consequently, permuting a single Sentinel predictor resulted in only a modest reduction in model performance, likely reflecting substantial redundancy among conventional remote-sensing features.

Unlike handcrafted variables, foundation-model embeddings consist of latent representations that do not have a direct ecological or biophysical interpretation (Brown et al., 2025b; Feng et al., 2026). Therefore, importance scores for individual embedding dimensions should not be interpreted as evidence that a small subset of channels alone drives

model performance. Moreover, permutation importance is sensitive to correlations among predictors and may underestimate the contribution of features whose information is shared across multiple dimensions. This limitation is particularly relevant for embedding spaces, where predictive information may be distributed across numerous latent channels.

The relatively gradual decline in importance values among the top-ranked embedding dimensions indicates that predictive information is not concentrated within a few dominant channels. Instead, multiple latent dimensions contributed at comparable levels to model performance, suggesting that the embeddings function as compact representations in which ecological information is encoded across several complementary features. Therefore, the importance analysis is most appropriately viewed as a tool for characterizing patterns of information distribution rather than for assigning ecological meaning to individual embedding dimensions. A more rigorous interpretation would require dedicated analyses such as embedding attribution, ablation experiments, gradient-based explanations, or transferability assessments across regions and years, which were beyond the scope of the present study.

5. Conclusion

This study introduced and evaluated a foundation-model embedding workflow for regional forest-diversity mapping and benchmarked its performance against comprehensive S1 and S2 handcrafted feature stacks across the Hyrcanian forest belt. Using a rigorous spatial cross-validation framework, foundation-model embeddings consistently achieved the highest predictive performance across all evaluated diversity indicators, with the largest gains observed for structural diversity. Among the evaluated embedding products, AEF consistently outperformed TESSERA and the conventional remote-sensing feature sets.

The results further revealed a clear hierarchy among the handcrafted predictors. S2-based feature sets provided competitive performance for taxonomic diversity mapping, whereas S1 predictors alone contributed little to no predictive value. Moreover, combining S1 and S2 features produced only marginal improvements over S-2 alone, suggesting that most of the useful information for diversity estimation in the Hyrcanian forests was contained within the optical observations.

Beyond overall accuracy, the embedding-based models demonstrated more stable performance across structurally diverse forest conditions and produced lower prediction errors for complex stands. However, these gains come at the cost of reduced interpretability, as the ecological meaning of individual embedding dimensions remains largely unknown. Future research should therefore focus on improving the interpretability of foundation-model representations and evaluating their transferability across forest types, ecological regions, and time periods.

From an operational perspective, foundation-model embeddings offer perhaps their greatest advantage in computational efficiency and implementation simplicity. Although they consistently matched or exceeded the performance of handcrafted predictor sets, they did so using substantially fewer input variables and without the need for complex feature-engineering workflows. The AEF and TESSERA embeddings reduced predictor dimensionality from several hundred multi-temporal Sentinel-derived variables to only 64 and 128 latent features, respectively, while maintaining superior predictive performance. This reduction simplifies data preparation, lowers storage and

computational requirements, and facilitates scalable deployment across large forested regions. While multi-temporal Sentinel-2 feature stacks remain attractive because of their ecological interpretability, embedding-based representations provide a more operationally efficient solution for large-scale forest diversity monitoring.**

Overall, the findings demonstrate that geospatial foundation-model embeddings represent a promising new generation of predictors for biodiversity monitoring and forest inventory applications, providing measurable improvements over conventional feature-engineering approaches in structurally complex, species-rich forests.

6. Acknowledgment

National Forest Inventory data used in this study were provided in part by the Organization of Natural Resources and Watershed Management of Iran, whose support is gratefully acknowledged. This work is based upon research funded by Iran National Science Foundation (INSF) under project No 40500432.

7. Declaration of generative AI and AI-assisted technologies in the manuscript preparation process

During the preparation of this work, the authors used ChatGPT and Gemini in order to polish the text and to debug the Python code. After using this tool, the authors reviewed and edited the content as needed and take full responsibility for the content of the published article.

8. Data availability

The field inventory data supporting the findings of this study are not publicly available because they are owned by the Natural Resources and Watershed Management Organization of Iran and cannot be shared without permission from the data provider. Access to these data is subject to institutional restrictions.

9. References

Akbari, H., Kalbi, S., 2019a. Modeling the diversity of tree species in circular forests using GeoEye images (Case study: Sari Gardeshi Series). Journal of Wood and Forest Science and Technology 26, 51–62. https://doi.org/10.22069/JWFST.2019.16391.1801

Akbari, H., Kalbi, S., 2019b. Tree species diversity monitoring using GeoEye satellite image in Gardeshi forest District. Journal of Wood and Forest Science and Technology 26, 51–62.

Akbari, H., Kalbi, S., 2016. Determining Pleiades satellite data capability for tree diversity modeling. IForest 10, 348. https://doi.org/10.3832/IFOR1884-009

Akhani, H., Djamali, M., Ghorbanalizadeh, A., And, E.R., 2010. Plant biodiversity of Hyrcanian relict forests, Iran: An overview of the flora, vegetation, palaeoecology and conservation. Pak. J. Bot. 42, 231–258.

Armston, J.D., Scarth, P., Lucas, R.M., Phinn, S., Dubayah, R., 2021. Comparison of spaceborne and airborne LiDAR for characterizing canopy structure and vegetation height. Remote Sens. Environ. 267, 112730. https://doi.org/10.1016/j.rse.2021.112730

Attarchi, S., Gloaguen, R., 2018. A multi-sensor approach for improving biodiversity estimation in the Hyrcanian mountain forest, Iran. Int. J. Remote Sens. 39, 7311–7327. https://doi.org/10.1080/01431161.2018.1468114;WGROUP:STRING:PUBLICATION

Attarchi, S., Gloaguen, R., 2013. Joint processing of Landsat ETM+ and ALOS-PALSAR data for species richness and forest biodiversity monitoring, in: Image and Signal Processing for Remote Sensing XIX. SPIE, p. 88920Y. https://doi.org/10.1117/12.2029328

Atzberger, C., Immitzer, M., Hemes, K.S., Kästenbauer, M., López, J., Terra, T., Rajadel-Lambistos, C., de Souza, S.F., Trabaquini, K., Wolff, N., 2025. A scalable, annual aboveground biomass product for monitoring carbon impacts of ecosystem restoration projects. Remote Sens. Environ. 327, 114774. https://doi.org/10.1016/j.rse.2025.114774

Brown, C.F., Kazmierski, M.R., Pasquarella, V.J., Rucklidge, W.J., Samsikova, M., Zhang, C., Shelhamer, E., Lahera, E., Wiles, O., Ilyushchenko, S., Gorelick, N., Zhang, L.L., Alj, S., Schechter, E., Askay, S., Guinan, O., Moore, R., Boukouvalas, A., Kohli, P., 2025a. AlphaEarth Foundations: An embedding field model for accurate and efficient global mapping from sparse label data. https://doi.org/10.48550/arXiv.2507.22291

Brown, C.F., Kazmierski, M.R., Pasquarella, V.J., Rucklidge, W.J., Samsikova, M., Zhang, C., Shelhamer, E., Lahera, E., Wiles, O., Ilyushchenko, S., Gorelick, N., Zhang, L.L., Alj, S., Schechter, E., Askay, S., Guinan, O., Moore, R., Boukouvalas, A., Kohli, P., 2025b. AlphaEarth Foundations: An embedding field model for accurate and efficient global mapping from sparse label data. https://doi.org/10.48550/arXiv.2507.22291

Daryaei, A., Lechner, M., Iglseder, A., Waser, L.T., Immitzer, M., 2025. Sentinel-2 vs. PlanetScope: Comparison and combination for tree species classification in two central European forest ecosystems. Remote Sens. Appl. 38, 101617. https://doi.org/10.1016/j.rsase.2025.101617

Delegido, J., Verrelst, J., Alonso, L., Moreno, J., 2011. Evaluation of Sentinel-2 Red-Edge Bands for Empirical Estimation of Green LAI and Chlorophyll Content. Sensors 11, 7063–7081. https://doi.org/10.3390/s110707063

Fassnacht, F.E., Latifi, H., Stereńczak, K., Modzelewska, A., Lefsky, M., Waser, L.T., Straub, C., Ghosh, A., 2016. Review of studies on tree species classification from remotely sensed data. Remote Sens. Environ. 186, 64–87. https://doi.org/10.1016/j.rse.2016.08.013

Fathi, M.R., Latifi, H., Gholizadeh, H., Khare, S., 2024. PaRaVis: An automatic Python graphical package for ensemble analysis of plant beta diversity using remote sensing proxies. Ecol. Inform. 82, 102739. https://doi.org/10.1016/J.ECOINF.2024.102739

Feng, Z., Atzberger, C., Jaffer, S., Knezevic, J., Sormunen, S., Young, R., Lisaius, M.C., Immitzer, M., Jackson, T., Ball, J., Coomes, D.A., Madhavapeddy, A., Blake, A., Keshav, S., 2026. TESSERA: Temporal Embeddings of Surface Spectra for Earth Representation and Analysis.

Frampton, W.J., Dash, J., Watmough, G., Milton, E.J., 2013. Evaluating the capabilities of Sentinel-2 for quantitative estimation of biophysical variables in vegetation. ISPRS Journal of Photogrammetry and Remote Sensing 82, 83–92. https://doi.org/10.1016/j.isprsjprs.2013.04.007

Ghaisaryan, A., Fatehi, P., Etemad, V., 2023. Estimation of species diversity in the Hyrcanian forests using Sentinel-2 Data (Case study: Kheyrud forest, Mazandaran). Forest and Wood Products 76, 229–243. https://doi.org/10.22059/JFWP.2023.362198.1261

Gotelli, N.J., Colwell, R.K., 2001. Quantifying biodiversity: procedures and pitfalls in the measurement and comparison of species richness. Ecol. Lett. 4, 379–391. https://doi.org/10.1046/j.1461-0248.2001.00230.x

Hashemi, S.A., Fallah Chai, M.M., Bayat, S., 2012. An analysis of vegetation indices in relation to tree species diversity using by satellite data in the northern forests of Iran. Arabian Journal of Geosciences 2012 6:9 6, 3363–3369. https://doi.org/10.1007/S12517-012-0576-8

Hoffmann, J., Muro, J., Dubovyk, O., 2022. Predicting Species and Structural Diversity of Temperate Forests with Satellite Remote Sensing and Deep Learning. Remote Sens. (Basel). 14, 1631. https://doi.org/10.3390/rs14071631

Homami Totmaj, L., Ramezani, E., Alizadeh, K., Behling, H., 2021. Four millennia of vegetation and environmental history above the Hyrcanian forest, northern Iran. Veg. Hist. Archaeobot. 30, 611–621. https://doi.org/10.1007/s00334-020-00813-y

Huete, A., Didan, K., Miura, T., Rodriguez, E.P., Gao, X., Ferreira, L.G., 2002. Overview of the radiometric and biophysical performance of the MODIS vegetation indices. Remote Sens. Environ. 83, 195–213. https://doi.org/10.1016/S0034-4257(02)00096-2

Immitzer, M., Neuwirth, M., Böck, S., Brenner, H., Vuolo, F., Atzberger, C., 2019. Optimal Input Features for Tree Species Classification in Central Europe Based on Multi-Temporal Sentinel-2 Data. Remote Sens. (Basel). 11, 2599. https://doi.org/10.3390/rs11222599

Immitzer, M., Vuolo, F., Atzberger, C., 2016. First Experience with Sentinel-2 Data for Crop and Tree Species Classifications in Central Europe. Remote Sens. (Basel). 8, 166. https://doi.org/10.3390/rs8030166

Jetz, W., McGeoch, M.A., Guralnick, R., Ferrier, S., Beck, J., Costello, M.J., Fernandez, M., Geller, G.N., Keil, P., Merow, C., Meyer, C., Muller-Karger, F.E., Pereira, H.M., Regan, E.C., Schmeller, D.S., Turak, E., 2019. Essential biodiversity variables for mapping and monitoring species populations. Nat. Ecol. Evol. https://doi.org/10.1038/s41559-019-0826-1

Jost, L., 2006. Entropy and diversity. Oikos 113, 363–375. https://doi.org/10.1111/j.2006.0030-1299.14714.x

Kacic, P., Kuenzer, C., 2022. Forest Biodiversity Monitoring Based on Remotely Sensed Spectral Diversity—A Review. Remote Sens. (Basel). 14, 5363. https://doi.org/10.3390/rs14215363

Lechner, M., Dostálová, A., Hollaus, M., Atzberger, C., Immitzer, M., 2022. Combination of Sentinel-1 and Sentinel-2 Data for Tree Species Classification in a Central European Biosphere Reserve. Remote Sens. (Basel). 14, 2687. https://doi.org/10.3390/rs14112687

Lisaius, M.C., Keshav, S., Blake, A., Atzberger, C., 2026. Embedding -based Crop Type Classification in the Groundnut Basin of Senegal.

Liu, X., Frey, J., Munteanu, C., Still, N., Koch, B., 2023. Mapping tree species diversity in temperate montane forests using Sentinel-1 and Sentinel-2 imagery and topography data. Remote Sens. Environ. 292, 113576. https://doi.org/10.1016/j.rse.2023.113576

Lu, S., Guo, J., Zimmer-Dauphinee, J.R., Nieusma, J.M., Wang, X., VanValkenburgh, P., Wernke, S.A., Huo, Y., 2025. Vision Foundation Models in Remote Sensing: A survey. IEEE Geosci. Remote Sens. Mag. 13, 190–215. https://doi.org/10.1109/MGRS.2025.3541952

MacArthur, R.H., MacArthur, J.W., 1961. On Bird Species Diversity. Ecology 42, 594–598. https://doi.org/10.2307/1932254

Misra, G., Cawkwell, F., Wingler, A., 2020. Status of Phenological Research Using Sentinel-2 Data: A Review. Remote Sens. (Basel). 12, 2760. https://doi.org/10.3390/rs12172760

Mohammadi, J., Shataee, S., 2010. Possibility investigation of tree diversity mapping using Landsat ETM+ data in the Hyrcanian forests of Iran. Remote Sens. Environ. 114, 1504–1512. https://doi.org/10.1016/J.RSE.2010.02.004

Mohammadi, J., Shataee, S., Babanezhad, M., 2011. Estimation of forest stand volume, tree density and biodiversity using Landsat ETM+Data, comparison of linear and regression tree analyses. Procedia Environ. Sci. 7, 299–304. https://doi.org/10.1016/j.proenv.2011.07.052

Mohammadi, J., Shataee, S., Næsset, E., 2020. Modeling tree species diversity by combining ALS data and digital aerial photogrammetry. Science of Remote Sensing 2, 100011. https://doi.org/10.1016/J.SRS.2020.100011

Mohite, J.D., Sawant, S.A., Pandit, A., Pappula, S., 2020. INVESTIGATING THE PERFORMANCE OF RANDOM FOREST AND SUPPORT VECTOR REGRESSION FOR ESTIMATION OF CLOUD-FREE NDVI USING SENTINEL-1 SAR DATA. The International Archives of the Photogrammetry, Remote Sensing and Spatial Information Sciences XLIII-B3-2020, 1379–1383. https://doi.org/10.5194/isprs-archives-XLIII-B3-2020-1379-2020

Muise, E.R., Andrew, M.E., Coops, N.C., Hermosilla, T., Burton, A.C., Ban, S.S., 2024. Disentangling linkages between satellite-derived indicators of forest structure and productivity for ecosystem monitoring. Sci. Rep. 14, 1–16. https://doi.org/10.1038/s41598-024-64615-2

Müller, W., 2019. The Hyrcanian Forests: An ancient ecosystem on the UNESCO World Heritage List. Global Ecology and Biodiversity 28, 1381–1393.

Pereira, H.M., Ferrier, S., Walters, M., Geller, G.N., Jongman, R.H.G., Scholes, R.J., Bruford, M.W., Brummitt, N., Butchart, S.H.M., Cardoso, A.C., Coops, N.C., Dulloo, E., Faith, D.P., Freyhof, J., Gregory, R.D., Heip, C., Höft, R., Hurtt, G., Jetz, W., Karp, D.S., McGeoch, M.A., Obura, D., Onoda, Y., Pettorelli, N., Reyers, B., Sayre, R., Scharlemann, J.P.W., Stuart, S.N., Turak, E., Walpole, M., Wegmann, M., 2013. Essential Biodiversity Variables. Science (1979). 339, 277–278. https://doi.org/10.1126/science.1229931

Poorazimy, M., Shataee, S., Aghababaei, H., Tomppo, E., Praks, J., 2023. First Demonstration of Space-Borne Polarization Coherence Tomography for Characterizing Hyrcanian Forest Structural Diversity. Remote Sensing 2023, Vol. 15, Page 555 15, 555. https://doi.org/10.3390/RS15030555

Ramezani, E., Marvie Mohadjer, M.R., Knapp, H.D., Ahmadi, H., Joosten, H., 2008. The late-Holocene vegetation history of the Central Caspian (Hyrcanian) forests of northern Iran. Holocene 18, 307–321. https://doi.org/10.1177/0959683607086768

Ramezani, E., Mrotzek, A., Marvie Mohadjer, M.R., Kakroodi, A.A., Kroonenberg, S.B., Joosten, H., 2016. Between the mountains and the sea: Late Holocene Caspian Sea level fluctuations and vegetation history of the lowland forests of northern Iran. Quaternary International 408, 52–64. https://doi.org/10.1016/j.quaint.2015.12.041

Ren, C., Jiang, H., Xi, Y., Liu, P., Li, H., 2023. Quantifying Temperate Forest Diversity by Integrating GEDI LiDAR and Multi-Temporal Sentinel-2 Imagery. Remote Sens. (Basel). 15. https://doi.org/10.3390/rs15020375

Roberts, D.R., Bahn, V., Ciuti, S., Boyce, M.S., Elith, J., Guillera-Arroita, G., Hauenstein, S., Lahoz-Monfort, J.J., Schröder, B., Thuiller, W., Warton, D.I., Wintle, B.A., Hartig, F., Dormann, C.F., 2017. Cross-validation strategies for data with temporal, spatial, hierarchical, or phylogenetic structure. Ecography 40, 913–929. https://doi.org/10.1111/ecog.02881

Sagheb Talebi, K., Sajedi, T., Pourhashemi, M., 2014. Forests of Iran, Springer, Plant and Vegetation. Springer Netherlands, Dordrecht. https://doi.org/https://doi.org/10.1007/978-94-007-7371-4

Schneider, F.D., Ferraz, A., Hancock, S., Duncanson, L.I., Dubayah, R.O., Pavlick, R.P., Schimel, D.S., 2020. Towards mapping the diversity of canopy structure from space with GEDI. Environmental Research Letters 15, 115006. https://doi.org/10.1088/1748-9326/ab9e99

Shannon, C.E., 1948. A Mathematical Theory of Communication. Bell System Technical Journal 27, 379–423. https://doi.org/10.1002/j.1538-7305.1948.tb01338.x

Sohrabi, H., 2025. Does UNESCO designation enhance forest protection? Evidence from the Hyrcanian national forest inventory. Trees, Forests and People 21, 100956. https://doi.org/10.1016/j.tfp.2025.100956

Sohrabi, H., Akhavan, R., 2026. Modeling structural attributes of Hyrcanian forests using spaceborne LiDAR, machine learning algorithms, and a hierarchical field data collection approach. For. Ecol. Manage. 599, 123287. https://doi.org/10.1016/j.foreco.2025.123287

Soleimannejad, L., Ullah, S., Abedi, R., Dees, M., Koch, B., 2019. Evaluating the potential of sentinel-2, landsat-8, and irs satellite images in tree species classification of hyrcanian forest of iran using random forest. Journal of Sustainable Forestry 38, 615–628. https://doi.org/10.1080/10549811.2019.1598443;PAGE:STRING:ARTICLE/CHAPTER

Szwarcman, D., Roy, S., Fraccaro, P., Gíslason, Þ.E., Blumenstiel, B., Ghosal, R., de Oliveira, P.H., Almeida, J.L. de S., Sedona, R., Kang, Y., Chakraborty, S., Wang, S., Gomes, C., Kumar, A., Truong, M., Godwin, D., Lee,

H., Hsu, C.-Y., Asanjan, A.A., Mujeci, B., Shidham, D., Keenan, T., Arevalo, P., Li, W., Alemohammad, H., Olofsson, P., Hain, C., Kennedy, R., Zadrozny, B., Bell, D., Cavallaro, G., Watson, C., Maskey, M., Ramachandran, R., Moreno, J.B., 2025. Prithvi-EO-2.0: A Versatile Multi-Temporal Foundation Model for Earth Observation Applications. https://doi.org/https://doi.org/10.48550/arXiv.

Teshager, Z., Soromessa, T., 2025. Forest Plant Diversity Assessment Based on Remote Sensing: A Systematic Literature Review. https://doi.org/10.21203/rs.3.rs-6105040/v1

Valavi, R., Elith, J., Lahoz-Monfort, J.J., Guillera-Arroita, G., 2019. blockCV: An r package for generating spatially or environmentally separated folds for k-fold cross-validation of species distribution models. Methods Ecol. Evol. 10, 225–232. https://doi.org/10.1111/2041-210X.13107

Xiao, A., Xuan, W., Wang, J., Huang, J., Tao, D., Lu, S., Yokoya, N., 2025. Foundation Models for Remote Sensing and Earth Observation: A survey. IEEE Geosci. Remote Sens. Mag. https://doi.org/10.1109/MGRS.2025.3576766

Yang, Q., Wang, L., Huang, J., Lu, L., Li, Y., Du, Y., Ling, F., 2022. Mapping Plant Diversity Based on Combined SENTINEL-1/2 Data—Opportunities for Subtropical Mountainous Forests. Remote Sens. (Basel). 14, 492. https://doi.org/10.3390/rs14030492

Zbontar, J., Jing, L., Misra, I., Lecun, Y., Deny, S., 2021. Barlow Twins: Self-Supervised Learning via Redundancy Reduction.